Heliyon 8 (2022) e12032

Contents lists available at ScienceDirect

Heliyon

journal homepage: www.cell.com/heliyon

Research article

Alginate/pectin dressing with niosomal mangosteen extract for enhanced wound healing: evaluating skin irritation by structure-activity relationship

Philaslak Pooprommin [a], Chawan Manaspon [b], Anupma Dwivedi [c], Anisha Mazumder [c], Surat Sangkaew [a], Smith Wanmasae [d], Jitbanjong Tangpong [d,e], Tassanee Ongtanasup [a], Komgrit Eawsakul [a,e,*]

[a] School of Medicine, Walailak University, Nakhon Si Thammarat 80160, Thailand
[b] Biomedical Engineering Institute, Chiang Mai University, Chiang Mai 50200, Thailand
[c] Faculty of Pharmacy, Charles University, Hradec Králové, Czech Republic
[d] School of Allied Health Sciences, Walailak University, Nakhon Si Thammarat 80160, Thailand
[e] Research Excellence Center for Innovation and Health Products (RECIHP), Walailak University, Nakhon Si Thammarat 80160, Thailand

ARTICLE INFO

Keywords:
Hydrogel
Niosome
Mangosteen extract
Skin irritation

ABSTRACT

Most modern wound dressings assist the wound-healing process. In contrast, conventional wound dressings have limited antibacterial activity and promote sporadic fibroblast growth. Therefore, wound dressings with prolonged substance release must be improved. This research aimed to develop hydrogel films. These were synthesized from alginate and pectin, incorporated with mangosteen extract (ME), and encapsulated in niosomes (ME-loaded niosomes). Subsequently, we examined the in vitro release and physical characteristics of ME-loaded niosomes. These characteristics included particle pH, size, charge, polydispersity index (PDI), and drug loading properties. These properties included drug loading content (DLC), entrapment efficiency (EE), and yield (Y). Additionally, we examined the swelling ratio and biological characteristics of the hydrogel film. These characteristics included antibacterial activity, cytotoxicity (L929), cell attachment to the tested materials, cell migration, hemocompatibility, and in vivo irritation. Significant results were obtained using a 2:1 niosome preparation containing Span60 and cholesterol. Ratio influenced size, charge, PDI, DLC, EE, and Y. The results were 225.5 ± 5.83 nm, negatively charged, 0.38, 16.2 ± 0.87%, 64.8 ± 3.49%, and 87.3 ± 3.09%, respectively. Additionally, the release of encapsulated ME was pH sensitive because 85% of the ME can be released at a pH of 5.5 within seven days and decrease to 70% at a pH of 7.4. The maximum swelling ratios of patches with 0.5% and 1% Ca^{2+} crosslinking were 867 wt% and 1,025 wt%, respectively, after 30 min. These results suggested that a medium dose (15 mg) of niosomal ME incorporated in a hydrogel film provided better bacterial inhibition, cell migration, and cell adhesion in an in vitro model. Additionally, no toxicity was observed in the fibroblasts and red blood cells. Therefore, given the above-mentioned advantages, this product can be a promising candidate for wound dressing applications.

1. Introduction

The skin is the largest organ in the body. It accounts for 15–20% of the whole-body mass. The skin tissue comprises three main layers: the epidermis, dermis, and hypodermis [1]. The dermal extracellular matrix (ECM) is an extensive molecular network comprising collagen, elastin, reticular fibers, and the dermis layer. Fibroblasts are primarily responsible for the production of collagen, proteoglycans, and glycosaminoglycans [2]. Skin defects, also known as wounds, are usually caused by thermal, physical, and chemical damage or physiological conditions [3]. Wound healing is a complex process chronologically comprising hemostasis, inflammation, proliferation, maturation, and differentiation. The prerequisites for an effective wound healing are a moist environment surrounding the wound [4], adequate oxygen circulation to promote cell regeneration [5] and absence of bacterial infection [6]. Products that accelerate wound healing have been widely used for wound dressing applications. Throughout the 1980s, numerous wound products have been developed by satisfying essential properties, such as

* Corresponding author.
E-mail address: Komgrit.ea@wu.ac.th (K. Eawsakul).

https://doi.org/10.1016/j.heliyon.2022.e12032
Received 4 August 2022; Received in revised form 28 September 2022; Accepted 24 November 2022

biocompatibility, non-cytotoxicity, non-immunogenicity, and stimulation of fibroblast and endothelial cell growth [7]. A suitable wound dressing absorbs excess exudates effectively. Although various types of wound dressing products are already available in the market, hydrogel-based wound dressings are still of interest to researchers and the market [8, 9]. Hydrogels are hydrophilic polymer matrices that absorb water and exudates from 10 to 1000 times their dry weights [10]. A hydrogel-based wound dressing creates a cooling surface to reduce pain [9] and maintains a moist environment to facilitate autolytic debridement of necrotic tissues [11]. It is pain-free, particularly when wound dressings are removed, due to the adhesion-free coverage of sensitive underlying tissues [9, 12].

Alginate is a polyanionic, hydrophilic, and natural polymer extracted from marine brown algae. It is generally regarded as an inexpensive, non-toxic, and biocompatible biomaterial [13]. It has been widely used in medical applications, such as tissue engineering, dental implantation, and wound dressing [14]. However, it has relatively poor mechanical properties. To address this, alginate is combined with pectin [15]. Pectin is a polyanionic and hydrophilic polymer extracted from fruit and vegetable pomaces. It has been extensively used in wound dressing [16]. The use of hybrid hydrogels derived from alginate and pectin (AP) has been considered for wound dressing applications [17]. Although these polymers are non-toxic and biocompatible, their antibacterial properties are not sufficient to prevent wound infection [18]. Wound dressings must have satisfactory antibacterial activity. In this study, mangosteen extract (ME) was used for skin infection treatment and wound healing; the ingredient has been used for centuries [19]. Additionally, it is effective against numerous bacterial (both gram positive and negative bacteria) and fungal infections [20] and has various other characteristics, such as anti-inflammatory, antioxidant, and anti-allergy properties [20, 21]. However, owing to ME has a short duration of bacterial inhibition. Thus, developing antibacterial substances is imperative for long-term bacterial inhibition. Using polymers as drug carriers allows for the sustained and controlled release of antibiotics to prevent long-term infections [22]. Niosomes, a subcategory of drug delivery carriers, present promising properties, such as high drug encapsulation efficiency and non-toxicity [23]. Niosomes are nonionic surfactant vesicular systems. Substances are loaded into the vesicles, which are fabricated by nonionic surfactants, such as Span or Tween, and cholesterol (cho) through the sonication method [24]. Niosomes have been used for various applications, such as targeted, sustained, and controlled release of substances [25].

To the best of our knowledge, this study was the first to examine the sustained release, antibacterial activity, and wound healing properties of ME-loaded niosomes incorporated into A/*P hydrogels*. A study showed that hydrogels made from hyaluronic acid and chitosan lacked homogeneity because deacetylated chitosan is insoluble [26]; however, all wound dressings were applied to the skin at a pH of 5.5. Due to the constraints of combined hyaluronic acid and chitosan, natural polymers, such as sodium alginate (SA) and pectin, were used in this study.

2. Materials and methods

2.1. Materials

Garcinia mangostana was obtained from Asia & Pacific Quality Trade Co., Ltd (Bangkok, Thailand); Chloroform, from Thai Public Oil Co., Ltd (Bangkok, Thailand); SA (CAS:9005-38-3), pectin (CAS:9000-69-5), and dimethyl sulfoxide, from Sigma–Aldrich; Mueller–Hinton agar (MHA) and trypticase soya agar, from Difco™, Becton Dickinson Co., and Spark (MD, USA); Dulbecco's modified Eagle's medium (DMEM), fetal bovine serum (FBS), 0.25% trypsin–ethylenediaminetetraacetic acid, trypan blue, phosphate-buffered saline (PBS), penicillin, streptomycin, 3-(4,5-dimethylthiazol-2-yl)-2,5-diphenyltetrazolium bromide (MTT), glycerin, Span™ 60, and cho, from Gibco (CA, USA); and all solvents, from RCI Labscan Ltd (Bangkok, Thailand).

2.2. Preparation of ME-loaded niosomes

2.2.1. ME extraction

G. mangostana Linn pericarps were collected, cleaned with tap water, and air-dried at room temperature at the RECIHP laboratory., The pericarps were dried in a hot air oven at 45 °C for three days and ground into a fine powder in a stainless steel jar blender (model no. BL-Y66S-1; Guangdong, China). The dried powder (100 g) was extracted with 500 mL deionized (DI) water in an autoclave at 105 °C and 15 psi for 60 min. The aqueous phase was filtered through Whatman No. 1 filter paper (Whatman International Ltd., Kent, UK). The filtered crude aqueous extract was lyophilized under vacuum at—80 °C for 18 h. The crude extract yield was 4.62%. The crude extract was stored at −30 °C until use.

2.2.2. Compound analysis by liquid chromatography–quadrupole time-of-flight mass spectrometry (LC–Q-TOF-MS)

The constitution of ME was evaluated by ultra-high performance LC, using a Zorbax Eclipse Plus C18 Rapid Resolution HD column (2.1 × 150 mm, 1.8 μm) and an LC-Q-TOF-MS apparatus to detect positive and negative electrospray ionization (ESI) mass spectra. The temperature was maintained at 40 °C. Mobile phase A comprised 0.1% formic acid in water, and mobile phase B comprised 11.5% acetonitrile solution. The elution steps were as follows [1]: 70% A and 30% B for 2 min [2], 5% A and 95% B for 14 min [3], 70% A and 30% B for 14.20 min, and [4] 70% A and 30% B for 20 min. The sample volume was 2 μL, with a flow rate of 0.2 mL/min. The drying gas temperature was set to 350 °C at 10 L/min; sheath gas temperature, to 275 °C; and nebulizer pressure, to 60 psig. Using a dual Agilent Jet Stream ESI source, we conducted LC–MS/MS in positive and negative ion modes, with a scanning range of 100–1500 m/z.

2.2.3. Probability of bioactivity in G. mangostana L. Compounds

Using the PASS online server (http://way2drug.com/PassOnline/), we predicted the bioactivity of the top-selected *G. mangostana* L. compounds. The categories of antibacterial and wound healing activities were considered for prediction purposes. The software forecasts the activity spectrum of a substance as either “probable activity (Pa)” or “probable inactivity (Pi).” The predictions are based on structure-activity relationships (SARs) [27].

2.2.4. Calibration of ME concentration

ME solution (45 mg/mL) was prepared in DI water and subjected to wavelength scanning using a UV spectrometer at 200–600 nm. The λmax of ME was 285 nm (Figure 1A). The freeze-dried ME extract was dissolved in DI water at various concentrations (0, 9, 18, 45, 150, and 300 mg/mL). Using a microplate reader (Tecan, Switzerland), we determined the standard curve of ME solution by measuring the absorbance at 285 nm (Figure 1B).

2.3. Antibacterial study of ME

The antibacterial activity of ME extracts was determined using the disk diffusion and broth dilution methods. The Kirby–Bauer disk diffusion method was used to determine the antibacterial activity of eight different concentrations of ME against *S. epidermidis* and *S. aureus* [28]. ME was briefly dissolved in normal saline solution (NSS) to obtain various concentrations (0.01, 0.03, 0.15, 0.3, 2.5, 5, 10, and 20 mg/mL). Four 6-mm blank disks containing 20 μL of each diluted ME extract solution were placed in plates seeded with different test bacteria. Vancomycin disks and disks impregnated with 20 μL of DI water were used as the positive (PC) and negative controls (NC), respectively. These were incubated for 24 h. Using ImageJ, we determined antibacterial activity by measuring the sizes of the zones of inhibition (ZOIs) and disk diameters in millimeters. The diameter of each disk was averaged from three ZOIs on different plates. A test extract with a ZOI ≥7 mm was

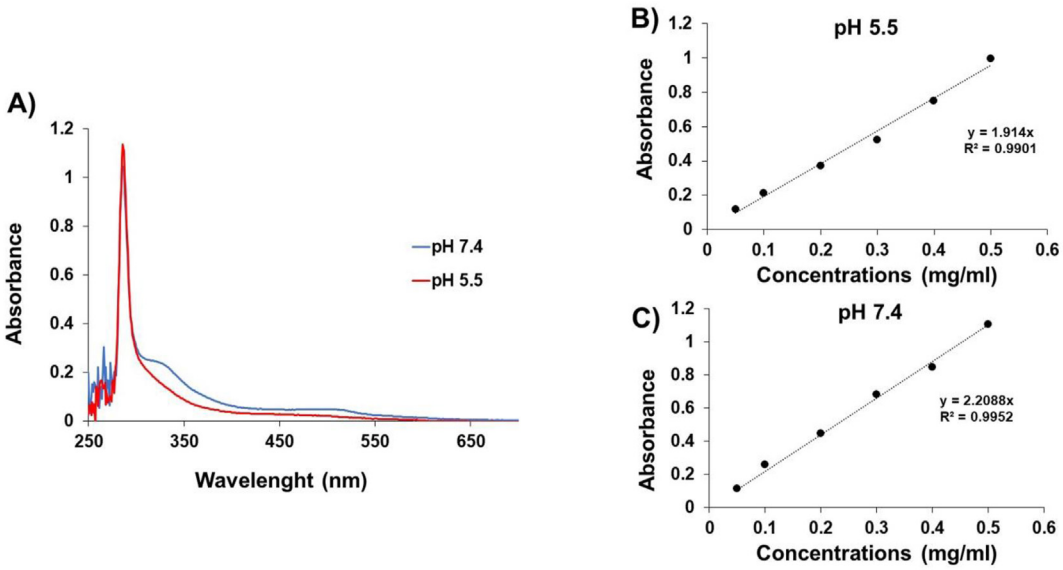

Figure 1. (A) UV absorption spectra of *G. mangostana* L. Pericarp extract at a pH of 5.5 (blue line) and 7.4 (red line). Standard curve of mangosteen extract at a pH of 5.5 (B) and 7.4 (C).

considered positive [29], While a ZOI of 0 was considered negative. Activity indices (Ais) were calculated by dividing the ZOI of ME by that of vancomycin. An AI >0.5 was considered a significant antibacterial activity [30].

Using eight different concentrations, the minimum inhibitory concentration (MIC) of ME against *S. aureus* and *S. epidermidis* was determined through the Clinical and Laboratory Standards Institute (2010–2012) broth microdilution method [31]. Mueller-Hinton broth was briefly used to dilute bacteria. A UV spectrophotometer was used at a wavelength of 600 nm and an optical density (OD) of 0.08–0.1 to quantify bacterial concentration (approximately 10^8 CFU/mL), and 10 μL of 10^8 CFU/mL bacteria was added to each well. The bacterial concentration in the final inoculum was 10^5 CFU/well. Eight two-fold serial dilutions of ME (100 μL) were added to the wells for the final high and low concentrations of 2.93 mg/mL and 0.02 mg/mL, respectively. Vancomycin and NSS were used as the PC and NC, respectively. After incubation at 37 °C for 24 h, pictures were captured before staining (Figure 2C, 1st and 3rd rows), and 10 μL of 0.005% resazurin was added to each well. To determine the MIC, antibacterial activity was examined at a λmax of 600 nm (blue) to determine the absence of viable bacteria [32, 33]. MEs with potentially therapeutic concentrations (changing from pink to blue) showed visible signs of antibacterial activity (MIC against the bacteria). All MIC values were averaged from six different plate readings. To determine the minimum bactericidal

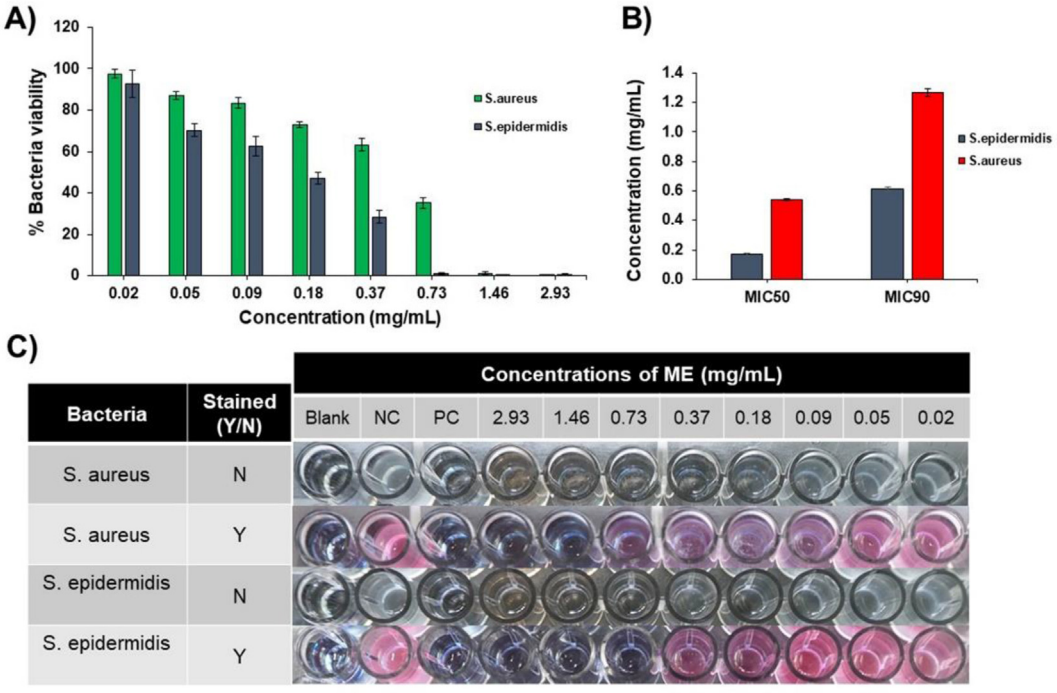

Figure 2. A) Percentage of bacterial viability. B) MIC_{50} and MIC_{90} of ME for *S. aureus* and *S. epidermidis*. C) Resazurin test to determine the MIC of ME.

concentration (MBC), concentrations higher than an MIC of 10 μL were dripped and spread on Mueller–Hinton agar plates to determine the absence of bacterial growth.

2.3.1. ME encapsulation in niosomes

Niosomes were prepared through a thin-film hydration process employing Span60 (S60) (a non-ionic surfactant) and cho [34]. First, several ratios of S60 and cho were dissolved in chloroform (2:1, 3:1, 4:1, and 5:1) (Table 4). After 15 min of agitation, the chloroform evaporated and left a thin-film coating on a glass vial. The blank niosomes were hydrated with DI water, while, ME-loaded niosomes were submerged in the ME solution (1 mg/mL) and agitated for 30 min. The niosomes were constructed by probe sonication for 30 s at an amplitude of 80% amplitude and temperature of 4 °C. The ME-loaded nisomes were investigated by fourier-transform infrared (FTIR) microspectroscopy to define the encapsulation of ME in niosomes.

2.4. Physical characterization of ME-loaded niosomes

2.4.1. Size, polydispersity index, and zeta potential

The niosomes were diluted (1:100) with DI water to remove the effects of multiple scattering and immediately inserted into the module. Droplet size was determined immediately after sample processing. Using Zetasizer Nano ZS (Malvern Panalytical, Malvern, UK), we measured the mean particle size and size distribution of the nanoparticles through the integrated light scattering method. Each nanoparticle preparation was evaluated in duplicate, with 30 measurements taken for each nanoparticle suspended in DI water. The mean particle size and polydispersity index were determined. The polydispersity index reflects the dispersion size in a monodisperse system, with values < 0.3 suggesting accurate measurements and high-quality colloids [35]. Each experiment was performed in triplicate. The tables and figures show the mean values for the three batches. The surface charge of the nanoparticles was assessed using Zetasizer Nano ZS and converted to zeta potential using the Smoluchowski equation [36]. The measurements were performed in an aqueous solution at a temperature of 25 °C.

2.4.2. ME entrapment efficiency

UV-visible spectroscopy was used to assess the quantity of ME in the niosomes. The newly synthesized niosome solution (10 mL) was purified by centrifugation at 3,000 rpm for 10 min and filtered through a 0.45-μm syringe filter to eliminate niosome aggregation [37]. The unencapsulated ME was removed through a centrifugal filter (MilliporeSigma, MA, USA) with a molecular weight cut-off of 50 kDa. The filter separated the drug-loaded micelles above from the unencapsulated ME below. The unencapsulated ME was collected and lyophilized. The lyophilized particles were dissolved in chloroform to determine the amount of ME in the particles. The Lyophilized micelles were weighed for quantification.

ME has an absorbance of 285 nm. The following equations were used to compute its drug attributes, such as DLC, EE, and Y [38, 39]:

$$\%\ \mathrm{DLC} = \frac{\text{amount of drug in a niosome}}{\text{theoretical amount of nanoparticles}} \times 100 \quad (1)$$

$$\%\ \mathrm{EE} = \frac{\text{amount of drug in a niosome}}{\text{initial amount of drug in the system}} \times 100 \quad (2)$$

$$\%\ \mathrm{Y} = \frac{\text{practical total amount of nanoparticles}}{\text{theoretical total amount of nanoparticles}} \times 100 \quad (3)$$

2.4.3. Evaluation of the in vitro release of ME from niosomes

Niosomes containing ME were placed in a dialysis bag (MWCO; Spectrum Labs, CA, USA) with a molecular weight cutoff of 15 kDa [40]. The bag was immersed in 25 ml PBS (pH 5.5 and 7.4) and incubated in an incubator shaker at a temperature of 37 °C and speed of 90 rpm [41, 42]. The PBS was replaced at regular intervals to maintain a sink condition. Using SwissADME (http://www.swissadme.ch/index.php), we calculated the sink condition by selecting the main constituents of ME, as previously identified by LC–Q-TOF-MS. A microplate reader was used to determine the drug release rate in the collected samples.

2.5. Preparation of ME-loaded niosomes incorporated in AP hydrogels

2.5.1. Synthesis of AP hydrogels

AP films were produced using a solvent casting method. A 1:1 ratio of SA and pectin was obtained by completely dissolving the particles in DI water at 900 rpm. Based on the weight of the SAP powder, 15% (w/w) glycerol was added as a plasticizer agent during the production process [43]. The solution was placed in an ultrasound machine for 15 min and degassed for 12 h. To create a SAP film with glycerol, 10 mL of the solution was poured onto Petri dishes with a diameter of 10 cm. The films were completely dried for two days at 55 °C with controlled humidity (50%). To form thin hydrogels with better mechanical strength, dry film samples with acceptable dimensions were cut and submerged for 30, 60, and 120 s in a 6 mL aqueous solution of 0.5% and 1% (w/v) $CaCl_2$. The hydrogels were cleaned with distilled water and dried at 55 °C until a constant weight was attained before use.

2.5.2. Preparation of ME-loaded niosomal AP patch

For niosomes (S60 and cho), a 2:1 ratio results in a high percentage of drug loading, yield, and encapsulation. Therefore, the ratio was chosen for the wound dressing formulation. To create the wound dressing, we used S60, cho, SA, pectin, glycerin, crude ME extract, and purified water. To create the formulation, we used glycerin to dissolve the crude extract. Glycerin is a non-toxic and highly biocompatible substance. It is frequently used in food, cosmetics, and pharmaceutical products. To prepare the SAP/ME films, an appropriate amount of ME solution was progressively added to the alginate solution until the final SAP/ME ratio of 85:15 (v/v) was reached [44]. The mixture was agitated at 600 rpm for 30 min and 10 mL was poured onto each Petri dish. The films were completely dried for two days at a temperature of 55 °C with controlled humidity (50%). Dry film samples with acceptable dimensions were cut and submerged for 30 s in a 6 mL aqueous solution of 1% (w/v) $CaCl_2$. The hydrogels were washed with distilled water and dried at 55 °C until a stable weight was attained before use.

2.6. Hydrogel characterization

2.6.1. Swelling ratio analysis

The swelling behavior of the SAP films was investigated at room temperature. Each film was submerged in separate containers of 5 mL PBS with a pH of 7.4. The samples were collected and rapidly blotted twice on a Kimwipe paper at 5, 10, 15, and 30 min and then weighed. The initial wet weight (Wo) and the succeeding wet weights (W) were recorded at predefined time intervals throughout the immersion experiment [45]. The swelling ratio was determined using Eq [4]. Three samples were evaluated for each group. The data are presented as means ± standard deviations.

$$\%\ \mathrm{swelling} = \frac{\mathrm{W} - \mathrm{Wo}}{\mathrm{Wo}} \times 100 \quad (4)$$

2.6.2. ME release study

Drug release was examined by immersing the ME-loaded SAP films (10 mg) in 25 mL PBS with a pH of 5.5 at 37 °C. To maintain the sink condition, the samples were removed at predefined time intervals and replaced with fresh PBS. Using SwissADME (http://www.swissadme.ch/index.php), we calculated the sink condition by selecting the main constituents of ME, as previously identified by LC–QTOF MS. A microplate reader was used to determine the amount of ME released at an absorbance of 286 nm. The trial was conducted in triplicate. Drug release was also tested in further experiments for the antibacterial study.

2.6.3. Antibacterial study

Antibacterial activity was evaluated using the broth dilution method. Mueller-Hinton broth was briefly used to dilute bacteria. A UV spectrophotometer was used at a wavelength of 600 nm and an OD of 0.08–0.1 to quantify bacterial concentration (approximately 10^8 CFU/mL), and 10 μL of 10^8 CFU/mL was added to each well. The bacterial concentration in the final inoculum was 10^5 CFU/well [46]. Vancomycin and NSS were used as the PC and NC, respectively. After the release of ME (100 μL), the wells were incubated for 24 h at 37 °C. Subsequently, pictures were captured before staining (Figure 2C, 1st and 3rd rows), and the MIC values were determined at different time points. Specifically, 10 μL of 0.005% resazurin was added to each well, and antibacterial activity was detected at a λmax of 600 nm to indicate the absence of viable bacteria (blue) [32, 33]. MEs released from SAP films with potentially therapeutic concentrations (changing from pink to blue) showed visible signs of antibacterial activity. All values were averaged from six different plate readings. The values indicated the duration of the SAP/ME patches' antibacterial effect.

2.6.4. Cell and sample preparation

A mouse fibroblast cell line (NCTC clone L929, IFO50409) was obtained from the Japanese Collection of Research Bioresources Cell Bank (Osaka, Japan). The cells were maintained in DMEM (Gibco, CA, USA) supplemented with 10% FBS (Gibco, CA, USA) and 1% (v/v) antibiotic–antimycotic solution (Gibco, CA, USA) at 37 °C under a 5% CO_2 atmosphere.

All samples (blank, 10, 15, and 20 mg ME-loaded membranes) were cut into 1 × 1 cm squares, sterilized under UV light for 1 h, washed with DI water, extracted according to ISO 10993 Part 12, and submerged in DMEM at 37 °C for 72 h. The collected (extracted) medium from each sample was filtered (Minisart® 0.2 μm cellulose acetate syringe filters; Sartorius, Göttingen, Germany) and stored at –20 °C until use.

2.6.5. Viability assays

The test was performed according to ISO 10993–5 [47]. L929 cells were seeded at a density of 10,000 cells/well in a 96-well plate and incubated for 24 h to allow for cell attachment. The culture medium was diluted with the extract to 100, 50, 25, and 10%. The cells were further maintained for 24 h before a quantitative MTT assay was performed [48]. To evaluate cell viability, the cells were incubated with 0.5 mg/mL of MTT solution (VWR Life Science, AMRESCO LLC, OH, USA) for 1 h at 37 °C. The insoluble formazan crystals were dissolved and measured using a microplate photometer (HiPo MPP-60; Biosan, Rīga, Latvia) at 568 nm. The cells that remained in the growth medium were used as the NC, whereas cells treated with 1% Triton X-100 in PBS (pH 7.4) for 15 min were used as the PC.

2.6.6. Cell morphology study

Sterilized membranes were used as substrates for cell attachment. L929 cells were directly seeded (10,000 cells/mL) onto the membranes in a 6-well plate. Sterilized glass coverslips were used as controls. After a 24-h r incubation, all samples were fixed with 3% glutaraldehyde (Sigma–Aldrich, MO, USA) for 15 min, dehydrated with an ethanol series [49, 50], and treated with hexamethyldisilazane (Sigma–Aldrich, MO, USA) for 5 min [51]. The samples were sputter-coated with gold and examined using a scanning electron microscope (SEM; JCM-7000; JEOL, Tokyo, Japan).

2.6.7. Cell migration assays

Cell migration was assessed in vitro through a scratch test [52, 53]. Cells were seeded at a density of 20,000 cells/well in 24-well plates and maintained in a standard growth media for 24 h. A scratch was created using a sterile pipette tip, and the cells were exposed to extracted mediums from distinct membranes (100%). Images were captured at 24 and 48 h, and ImageJ was used to quantify cell migration.

2.6.8. Hemocompatibility

Hemocompatibility was assessed through a complete blood count. A normal red blood cell (RBC) scattergram flag was detected by the HA3 Hematology Analyzer (BioSystems S.A., Barcelona, Spain) (Figure 12). RBC hemolysis can be quantified from a normal RBC count. RBCs were adjusted to equal concentrations before being tested with NSS. DI water was used as the PC. Patches containing different doses of ME (10, 15, and 20 mg) were extracted according to ISO10993-12 [54]. The extracted substances were incubated with the prepared RBCs. Previously, WUEC-22-158-01 was approved by the Internal Review Board (IRB) of the Center of Ethic Reinforcement for Human Research at Walailak University.

2.6.9. In vivo skin irritation study

The in vivo study was conducted at an ISO 17025-certified National Institute of Health Laboratory in Thailand. The study protocol was approved by the Animal Ethics Committee of Walailak University (protocol no. WU-ACUC-65044). The protocol complied with ISO 10993–10 [55]. We used three healthy, young female New Zealand white rabbits. Their body weights ranged from 2,000 to 3,000 g, in compliance with the OECD Guidelines for the Testing of Chemicals (Test no. 404) [56]. Animals from production sites undergo veterinary health assessments in conventional sanitary systems. At least 24 h before the test, the rabbits' fur on the back was shaved with a clipper, from the shoulder blades down to the line parallel to the lower spine (approximately 2.5 cm). The approximate width and length were 15 cm and 10 cm, respectively. Hydrogel films containing ME were cut to a size of 2.5 × 2.5 cm^2 and a thickness of no more than 0.5 mm, and their surfaces were smoothened. The rabbits had normal skin conditions and no scars, and they had not undergone other tests. After preparing a test animal, four test patches were taken and covered with adhesive tape. These were tightly wrapped around the body with a stretchable fabric and then wrapped with a transparent plaster to prevent sliding. After 4 h, all test patches were removed. The sample that remained on the test skin was gently wiped with distilled water several times and then allowed to dry. Abnormalities were observed in the area covered by the test patches at 1, 24, 48, and 72 h. The results and scores were recorded, and the primary irritation index was calculated. The scoring and reading criteria were based on skin redness (erythema and eschar formation) and edema formation.

2.7. Statistical analysis

All experiments were conducted in triplicate, and the results are presented as means ± SDs. Analysis of variance was performed using SPSS Statistics 17.0. Statistical significance was set at $P < 0.05$.

3. Results and discussion

3.1. Analysis of the chemical constituents and biological activities of G. Mangostana L

We performed LC–Q-TOF-MS in the positive and negative modes to qualitatively and quantitatively investigate the chemical components of ME. The corresponding SARs revealed the chemical constituents and bioactivity of ME. The area under the curve identified phenolic compounds, quinones, sugars, and xanthones as the principal ingredients of the top five ME extracts (Tables 1 and 2). The most significant −ESI compounds were 1) threo-isocitric acid (retention time [RT] = 2.092 min), which accounted for 7.48% of all ESI compounds; 2) epicatechin and 2-methoxy-1,4-benzoquinone (RT = 10.675 min), 6.85%; 3) procyanidin B2 (RT = 10.073 min), 5.86%; 4) quinic acid (RT = 2.305 min), 3.14%; and 5) catechin (RT = 9.684 min), 2.45%. Meanwhile, the most significant + ESI compound was palmitic amide (RT = 20.696 min) at 11.46%. Using the SAR method, we evaluated the structural formulae of these compounds and compared with their

Table 1. Characterization of *G. mangostana* L. compounds by LC-QTOF-MS in the −ESI mode.

No.	Name	Formula	RT	m/z
1	Galactaric acid	$C_6H_{10}O_8$	1.916	209.0303
2	D-Glucose 6-sulfate	$C_6H_{12}O_9S$	1.953	259.0129
3	L-Altruronic acid	$C_6H_{10}O_7$	2.041	193.0353
4	Galactonic acid	$C_6H_{12}O_7$	2.066	195.0513
5	Threo-Isocitric acid	$C_6H_8O_7$	2.092	191.0199
6	Quinic acid	$C_7H_{12}O_6$	2.305	191.0563
7	Oxalosuccinic acid	$C_6H_6O_7$	2.468	189.0042
8	Homoisocitrate	$C_7H_{10}O_7$	2.618	205.0353
9	Sucrose	$C_{12}H_{22}O_{11}$	2.618	341.1089
10	Coriose	$C_7H_{14}O_7$	2.643	209.0666
11	Maleic acid	$C_4H_4O_4$	2.819	115.0037
12	Malic acid	$C_4H_6O_5$	2.869	133.0143
13	Arabinopyranobiose	$C_{10}H_{18}O_9$	2.995	281.0876
14	Shikimic acid	$C_7H_{10}O_5$	3.02	173.0455
15	D-Galactopyranosyl-(1->3)-D-galactopyranosyl-(1->3)-L-arabinose	$C_{17}H_{30}O_{15}$	3.12	473.1506
16	3-Furoic acid	$C_5H_4O_3$	3.597	111.0088
17	Citric acid	$C_6H_8O_7$	4.626	191.02
18	Ascladiol	$C_7H_8O_4$	4.727	155.035
19	2,5-Dimethyl-3(2H)-furanone	$C_6H_8O_2$	5.003	111.0452
20	Phthalate 3,4-cis-dihydrodiol	$C_8H_8O_6$	5.053	199.0246
21	Methyl-2-alpha-L-fucopyranosyl-beta-D-galactoside	$C_{13}H_{24}O_{10}$	5.429	339.1295
22	Isopropyl apiosylglucoside	$C_{14}H_{26}O_{10}$	6.032	353.145
23	3-Glucosyl-2,3′,4,4′,6-pentahydroxybenzophenone	$C_{19}H_{20}O_{11}$	7.914	423.0936
24	Pyrocatechol	$C_6H_6O_2$	8.015	109.0296
25	2,6-dihydroxybenzoic acid	$C_7H_6O_4$	8.04	153.0192
26	Cynaroside A	$C_{21}H_{32}O_{10}$	8.441	443.1919
27	(-)-epicatechin-3′-O-glucuronide	$C_{21}H_{24}O_{11}$	8.742	451.1235
28	Chlorogenic Acid	$C_{16}H_{18}O_9$	9.345	353.0875
29	3,4-Dihydroxybenzaldehyde	$C_7H_6O_3$	9.521	137.024
30	(±)-Catechin	$C_{15}H_{14}O_6$	9.684	289.0718
31	Procyanidin B2	$C_{30}H_{26}O_{12}$	10.073	577.1349
32	Verbasoside	$C_{20}H_{30}O_{12}$	10.223	461.1659
33	Khellol glucoside	$C_{19}H_{20}O_{10}$	10.424	407.0981
34	Coriandrone C	$C_{13}H_{10}O_5$	10.449	245.0456
35	2-Methoxy-1,4-benzoquinone	$C_7H_6O_3$	10.675	137.0242
36	Epicatechin	$C_{15}H_{14}O_6$	10.675	289.0721
37	Marmesin	$C_{14}H_{14}O_4$	10.7	245.0818
38	Vanillin 4-sulfate	$C_9H_{10}O_6S$	10.851	245.0125
39	2-Acetyl-5,8-dihydroxy-3-methoxy-1,4-naphthoquinone	$C_{13}H_{10}O_6$	11.127	261.0406
40	Epifisetinidol-(4beta->8)-catechin	$C_{30}H_{26}O_{11}$	11.227	561.1399
41	4-O-8′,5′-5″-Dehydrotriferulic acid	$C_{30}H_{26}O_{12}$	11.629	577.1342
42	Garcimangosone D	$C_{19}H_{20}O_9$	11.83	391.1031
43	Amaroswerin	$C_{29}H_{30}O_{14}$	12.381	601.1585
44	O-Demethylfonsecin	$C_{14}H_{12}O_6$	12.733	275.056
45	Miscanthoside	$C_{21}H_{22}O_{11}$	12.846	449.1086
46	Streptonigrin	$C_{25}H_{22}N_4O_8$	12.997	505.1381
47	Citrusin B	$C_{27}H_{36}O_{13}$	13.235	567.2076
48	(R)-1-O-[b-D-Glucopyranosyl-(1->6)-b-D-glucopyranoside]-1,3-octanediol	$C_{20}H_{38}O_{12}$	14.038	469.2286
49	Urolithin D	$C_{13}H_8O_6$	16.046	259.0245
50	Coriandrin	$C_{13}H_{10}O_4$	18.054	229.0508
51	Muscomin	$C_{18}H_{18}O_7$	19.008	345.0978
52	(2S,4S,6S)-2-[2-(4-Hydroxy-3-meyhoxyphenyl)ethyl]tetrahydro-6-(4,5-dihydroxy-3-methoxyphenyl)-2H-pyran-4-yl 4-acetate	$C_{23}H_{28}O_8$	20.163	431.1705
53	Cubebininolide	$C_{24}H_{30}O_8$	21.417	445.1861
54	Ugaxanthone	$C_{18}H_{16}O_6$	24.781	327.0874
55	Garcinone C	$C_{23}H_{26}O_7$	26.989	413.1602
56	1,4,6-Trihydroxy-5-methoxy-7-prenylxanthone	$C_{19}H_{18}O_6$	27.441	341.1025
57	1-Isomangostin hydrate	$C_{24}H_{28}O_7$	27.993	427.1759
58	Garcinone A	$C_{23}H_{24}O_5$	33.364	379.1549
59	Dulciol C	$C_{28}H_{34}O_7$	33.515	481.2223
60	BR-Xanthone A	$C_{23}H_{24}O_6$	34.669	395.1499
61	α-Mangostin	$C_{24}H_{26}O_6$	35.121	409.1657
62	Dulciol B	$C_{28}H_{32}O_6$	35.987	463.2124

antibacterial and wound healing efficacies (Table 3). Given a Pa value > 0.7, threo-isocitric acid and palmitic amide reduced bacterial growth by inhibiting pseudolysin, as in previous studies [57, 58]. This showed that threo-isocitric acid and palmitic amide suppressed antimicrobial resistance and biofilms. Meanwhile, 2-methoxy-1,4-benzoquinone and quinic acid promoted wound healing through anti-inflammatory effects. Numerous studies [59, 60] have reported that quinones have antiviral, anti-ulcer, antitumor, and anti-inflammatory properties. Due to these, quinones have been used as scaffolds [61] to promote cell growth. Additionally, procyanidin B2 exhibited antihemorrhagic properties. It promoted the angiogenic activity of endothelial progenitor cells and wound healing in diabetic mice [62]. Specifically, procyanidin B2 protected the angiogenic activity, survival, and migration of endothelial progenitor cells by eliminating high glucose-induced oxidative stress and its corresponding damage. These mechanistic results depended on Nrf2 activation. Lastly, catechin and epicatechin exhibited antioxidant and antihistamine properties, respectively. Using an in vivo model, a previous study [63] evaluated the effects of catechin and epicatechin on scar formation in full-thickness incision wound healing. Both chemicals significantly improved the quality of scar formation in terms of collagen fiber growth and arrangement and increased the number of new blood vessels.

3.2. ME concentration standard curve

We used a scanning spectrogram with a step length of 1 nm to determine the detection wavelength of the ME in a universal microplate reader (Figure 1A). The absorbance varied with the pH of the surrounding environment. At a pH of 7.4, ME exhibited absorbance at 285 nm. At a pH of 5.5, ME exhibited absorbance at 286 nm. Thus, the detection wavelengths of ME were 285 and 286 nm, respectively [64, 65]. The universal microplate reader has the analytical power to simultaneously detect multiple samples. For example, an ultraviolet spectrophotometer can simultaneously detect a maximum of three samples, making it unsuitable for large samples. Large samples cause random and systematic errors that result in poor reproducibility and stability of experimental data [66].

In contrast, a universal microplate reader can simultaneously detect hundreds of samples. It utilizes a vertical rather than a horizontal optical path, creating a shorter light path than that of the UV spectrophotometer. This helps reduce detection errors [67, 68]. A calibration curve was created by plotting a graph of absorbance versus ME concentration (0.05–0.5 mg/mL) (Figures 1B and 1C). Six concentrations were used, and each concentration was analyzed in triplicate. The regression equation for ME was constructed using the least squares method (Figures 1B and 1C), where y represents the absorbance value of ME, while x represents the concentration of ME in mg/L. The linear correlation coefficient (R^2) was 1.0000 (n = 6) [69].

Table 2. Characterization of *G. mangostana* L. compounds by LC-QTOF-MS in the +ESI mode.

No.	Name	Formula	RT	m/z
1	Choline	$C_5H_{14}NO$	1.898	104.1073
2	6-(alpha-D-Glucosaminyl)-1D-myo-inositol	$C_{12}H_{23}NO_{10}$	1.947	342.1394
3	Trimethylammonioacetate	$C_5H_{12}\ NO_2$	2.023	118.0863
4	α-D-Glucose	$C_6H_{12}O_6$	2.023	203.0525
5	Maltose	$C_{12}H_{22}O_{11}$	2.199	365.1058
6	Trigonelline	$C_7H_8NO_2$	2.199	138.0552
7	Valiolone	$C_7H_{12}O_6$	2.299	215.0527
8	Firocoxib	$C_{17}H_{20}O_5S$	2.324	337.1103
9	Malonylcarnitine	$C_{10}H_{18}NO_6$	2.449	248.113
10	Sucrose	$C_{12}H_{22}O_{11}$	2.5	365.1056
11	2-(beta-D-Glucosyl)-sn-glycerol	$C_9H_{18}O_8$	2.751	277.0894
12	(-)-Dioxibrassinin	$C_{11}H_{12}N_2O_2S_2$	2.801	306.9967
13	Galactose-beta-1,4-xylose	$C_{11}H_{20}O_{10}$	3.102	335.0946
14	Adenine	$C_5H_5N_5$	3.504	136.0615
15	4-Guanidinobutanoic acid	$C_5H_{11}N_3O_2$	3.529	146.0923
16	D-Galactopyranosyl-(1->3)-D-galactopyranosyl-(1->3)-L-arabinose	$C_{17}H_{30}O_{15}$	4.508	497.1468
17	DL-o-Tyrosine	$C_9H_{11}NO_3$	4.633	182.0808
18	Cystine	$C_6H_{12}N_2O_4S_2$	4.658	241.0317
19	Ethyl beta-D-glucopyranoside	$C_8H_{16}O_6$	4.658	231.0839
20	(R)-N-Methylsalsolinol	$C_{11}H_{15}NO_2$	4.934	194.1175
21	2′-Aminoacetophenone	C_8H_9NO	4.959	136.0754
22	Kojic Acid	$C_6H_6O_4$	5.135	143.0338
23	2,3-Butanediol glucoside	$C_{10}H_{20}O_7$	5.211	275.1102
24	Methyl-2-alpha-L-fucopyranosyl-beta-D-galactoside	$C_{13}H_{24}O_{10}$	5.361	363.1256
25	Isopropyl beta-D-glucoside	$C_9H_{18}O_6$	5.713	245.0994
26	Isopropyl apiosylglucoside	$C_{14}H_{26}O_{10}$	5.988	377.1414
27	Leonuriside A	$C_{14}H_{20}O_9$	6.34	355.0997
28	Cynaroside A	$C_{21}H_{32}O_{10}$	8.473	467.188
29	3-Hydroxycoumarin	$C_9H_6O_3$	9.327	163.039
30	2-[4-(3-Hydroxypropyl)-2-methoxyphenoxy]-1,3-propanediol 1-glucoside	$C_{19}H_{30}O_{10}$	9.351	441.1727
31	Procyanidin B2	$C_{30}H_{26}O_{12}$	10.029	579.1502
32	Procyanidin B3	$C_{30}H_{26}O_{12}$	10.054	601.1311
33	*Phenylethyl primeveroside*	$C_{19}H_{28}O_{10}$	10.23	439.1569
34	Epicatechin	$C_{15}H_{14}O_6$	10.657	291.0866
35	cis-3,4-Leucopelargonidin	$C_{15}H_{14}O_6$	10.681	313.0682
36	2-Methoxy-1,4-benzoquinone	$C_7H_6O_3$	10.682	139.039
37	Epifisetinidol-(4beta->8)-catechin	$C_{30}H_{26}O_{11}$	11.234	563.1539
38	Unshuoside A	$C_{16}H_{28}O_7$	13.041	355.1724
39	Isolariciresinol 9-O-beta-D-glucoside	$C_{26}H_{34}O_{11}$	13.242	545.1987
40	2,6 dimethylheptanoyl carnitine	$C_{16}H_{32}NO_4$	13.668	302.2326
41	S-Furanopetasitin	$C_{24}\ H_{32}O_5S$	13.945	433.204
42	Hulupinic acid	$C_{15}H_{20}O_4$	16.379	287.1254
43	Palmitic amide	$C_{16}H_{33}NO$	20.696	256.2633
44	C16 Sphinganine	$C_{16}H_{35}NO_2$	20.721	274.2754
45	Alpha-CEHC	$C_{16}H_{22}O_4$	32.742	301.141
46	α-Mangostin	$C_{24}H_{26}O_6$	35.127	411.1804
47	Isoartocarpesin	$C_{20}H_{18}O_6$	35.177	355.1176

3.3. Antibacterial study of ME

ME was effective against *S. aureus* and *S. epidermidis*, as shown by the MIC and MBC values. These investigations employed various ME concentrations from 0.02 to 2.93 mg/mL (Figure 2A). The MIC_{50} and MIC_{90} concentrations of ME extract against *S. aureus* were 0.54 ± 0.01 and 1.27 ± 0.03 mg/mL, respectively (Figure 2B). The MIC_{50} and MIC_{90} values of ME against *S. epidermidis* were 0.17 ± 0.01 and 0.61 ± 0.02 mg/mL, respectively. These results showed that ME can inhibit *S. epidermidis* better than *S. aureus* because a lower ME concentration was used against *S. epidermidis*. However, the patch requires a sufficient ME concentration (a minimum concentration of 1.27 mg/mL) to suppress both the growth of both bacteria.

In addition, the antibacterial activity of ME was examined using the agar diffusion method. Figure 3 summarizes the results obtained from the corresponding ZOIs. The agar diffusion method measures the width of a substance that can inhibit bacteria. Generally, the size of the ZOI increased with antibacterial property. The NCs included the same components as the tested samples, except for ME. MEs with doses <0.15 and 0.3 mg did not inhibit *S. aureus* and *S. epidermidis*, respectively. Meanwhile, 20 mg ME inhibited *S. aureus* and *S. epidermidis*, with ZOIs reaching 17 ± 1.1 mm and 16 ± 1.2 mm, respectively. These findings demonstrated that ME concentration increased with antibacterial activity. However, excessive levels of ME have detrimental effects on fibroblasts (L929). Lower concentrations of ME were optimal for bacterial growth inhibition. The optimal AI value was [30] >0.5. *S. aureus* (AIs = 0.64) and *S. epidermidis* (AIs = 0.52) were suppressed by 2.5 mg ME.

Table 3. Pa and Pi values of phytochemical *G. mangostana* L. for antibacterial and wound healing predicted using the PASS online server.

No.	Compounds	Pa	Pi	Activities
1	Threo-isocitric acid	0.800	0.006	Pseudolysin inhibitor
2	Epicatechin	0.791	0.003	Histamine release inhibitor
3	2-methoxy-1,4-benzoquinone	0.743	0.011	Anti-inflammatory
4	Procyanidin B2	0.884	0.002	Antihemorrhagic
5	Quinic acid	0.705	0.015	Anti-inflammatory
6	Catechin	0.810	0.003	Antioxidant
7	Palmitic amide	0.802	0.006	Pseudolysin inhibitor

Table 4. Blank niosomes.

S60: Cho	Size (nm) ± SD	PDI	Zeta potential (mV)	%DL	%EE	% Yield
2: 1	202.7 ± 2.46	0.46	-25.9	n/a	n/a	88.9 ± 6.94
3: 1	223.1 ± 2.43	0.38	-53.1	n/a	n/a	91.7 ± 3.09
4: 1	225.7 ± 3.66	0.39	-53.3	n/a	n/a	93.3 ± 2.45
5: 1	212.6 ± 3.77	0.28	-42.1	n/a	n/a	88.9 ± 4.99

Data of mean +SD of 3 independent experiments.

3.4. Characterization of ME-loaded niosomes

We investigated the effects of different S60 and cho ratios (Table 4). The ME-loaded niosomes are presented in Table 5. FTIR was performed to examine the possible interactions between ME and niosomal components (Figure 4). Previous studies that used 2 to 5 parts S60 demonstrated that the proportion of S60 increased with size and % Y. A 4:1 S60 and cho ratio showed the highest % Y. However, % Y values decreased with the addition of S60 to ME-loaded niosomes. A 2:1 ratio of S60 and cho was selected because it showed the highest % Y while preserving ME content and a low PDI This indicated that the particle sizes of ME in this study were similar to those reported in another study [70]. These results concluded that a high percentage of S60 increased % Y and DLC values; however, if S60 exceeds 4 parts, the excess niosomes will produce the lowest % Y [71]. This may be explained by the presence of multiple bonds, which result in chain bending and alteration in molecular packing conditions [72]. In this study, the niosomal membrane exhibited increased permeability [73], which explained why excessive S60 in niosomes resulted in the lowest % Y. Therefore a lower percentage of S60 also resulted in a higher % Y and % DLC (Table 5).

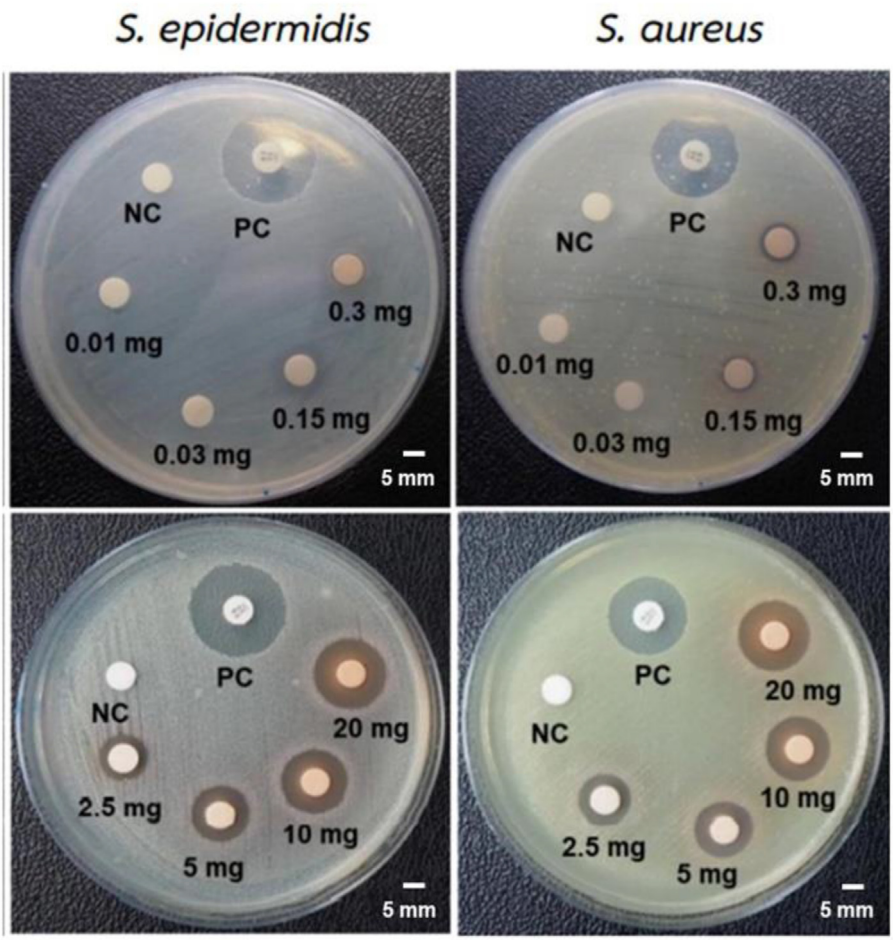

Figure 3. Disk diffusion (ZOI) results for *S. epidermidis* (left) and *S. aureus* (right): Vancomycin as the PC, NSS as the NC, and different concentrations of ME.

Table 5. ME-loaded niosomes.

S60: Cho: ME	Size (nm) ± SD	PDI	Zeta potential (mV)	%DL	%EE	% Yield
2: 1: 1	214.2 ± 9.0	0.23	-43.0	16.2 ± 0.87	64.8 ± 3.49	87.3 ± 3.09
3: 1: 1	358.5 ± 14.3	0.44	-35.0	13.7 ± 0.05	68.5 ± 0.26	53.0 ± 2.45
4: 1: 1	282.8 ± 10.2	0.44	-32.0	11.7 ± 0.25	70.24 ± 1.50	52.7 ± 2.49
5: 1: 1	353.6 ± 9.9	0.46	-30.1	9.8 ± 0.19	68.91 ± 1.33	50.0 ± 8.16

Data of mean ± SD of 3 independent experiments.

3.5. Characterization by FTIR

FTIR spectroscopy was performed to examine the chemical composition of ME, niosomal surface, and entrapment of ME in niosomes. Figure 4 shows the FTIR spectra of the ME extracts (green line). Numerous stretching vibration bands linked to organic functional groups were readily apparent in all observed spectra. At 3,274 cm^{-1}, 1,608 cm^{-1}, 1,442 cm^{-1}, 1,060 cm^{-1}, and 675 cm^{-1}, the round-shaped bands correspond to the vibrations of the O–H of alcohol, alkanes, C=O and C–O stretching, C–C, and the C=C of alkene [74]. As in the previous UV-visible spectrometry, the presence of phenolic arenes and polycyclic aromatic hydrocarbons with two or more rings were confirmed. This indicated the presence of cyanidin-3-sophoroside [74]. Many other compounds, such as quinones and xanthones, were identified (Tables 1 and 2).

Figure 4 illustrates the FTIR spectrum of freeze-dried niosome powder (red). All peaks associated with cho and S60 were present in the niosome spectra. Additional peaks that were not apparent in the cho or S60 spectra were also observed. The cho spectra revealed C–O stretching (1,060 cm^{-1}), C–H bond stretching (2,952 cm^{-1}), C–H bond bending (1,373 cm^{-1}), and –OH stretching (a wide peak at 3000–3700 cm^{-1}). The S60 spectra revealed C=O stretching (1,731 cm^{-1}); -C–CO–O- (1,180 cm^{-1}); aliphatic C–H stretching; and asymmetric, symmetric, and aliphatic (2,914 cm^{-1}, 2,852 cm^{-1}, and 723 cm^{-1}, respectively) –CH2- rocking (723 cm^{-1}). ME-loaded niosomes were used to illustrate the peaks of ME. Lacking peaks in ME upon being loaded into niosomes indicated that ME was successfully loaded into niosomes. Significant hydrogen bonding across formulation components was attributed to the extremely wide peak at 3,000–3,700 cm^{-1}. According to previous investigations, hydrogen bonds are more likely to form among ME, cho, and S60 [75,76].

3.6. Release of ME from niosomes

In studying the solubility of drug constituents, drug release is essential to sink condition. The maximum water solubility should not be

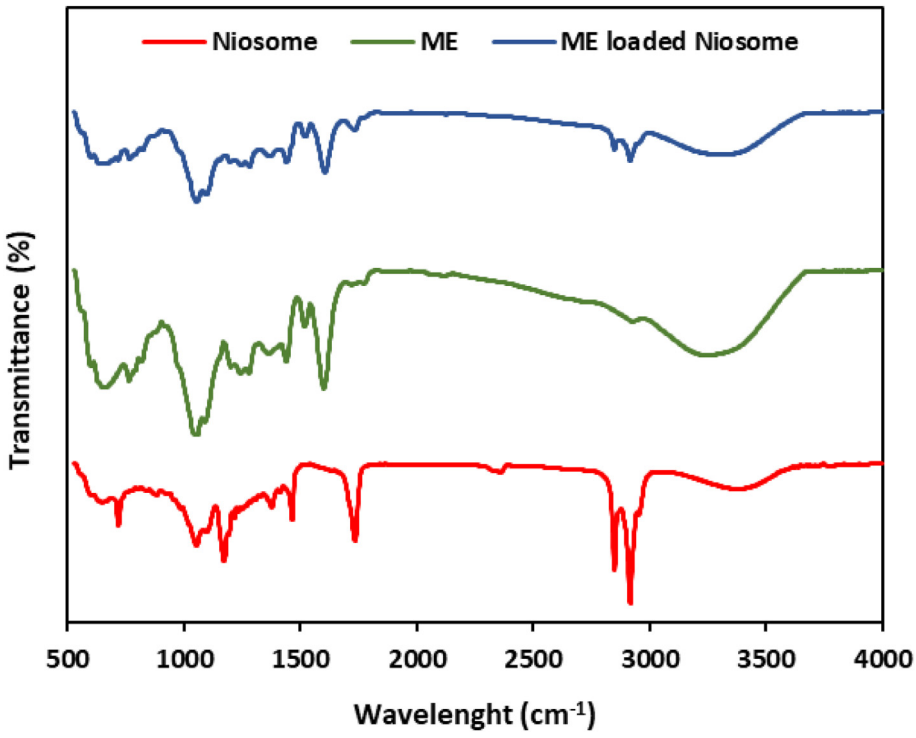

Figure 4. ATR-FTIR spectra of niosomes (red line), ME (green line), and ME-loaded niosomes (blue line).

Table 6. Main compounds of ME and their water solubility properties.

No.	Compounds	Percent containing	Solubility (mg/mL)
1	Palmitic amide	11.46%	6.31×10^{-3}
2	Threo-isocitric acid	7.48%	5.20×10^{2}
3	Epicatechin	6.85 %	1.74
4	2-methoxy-1,4-benzoquinone	6.85 %	35.3
5	Procyanidin B2	5.86%	4.15×10^{-3}
6	Quinic acid	3.14%	6.48×10^{2}
7	Catechin	2.45%	1.74

reached during drug release. The sink condition of each substance was calculated using SwissADME (http://www.swissadme.ch/index.php) (Table 6). The least soluble substance was procyanidin B2, with a solubility of 4.15×10^{-3} mg/mL in water. In this study, we used 25 mL PBS. In this regard, the maximum amount of procyanidin B2 in the total solution was 0.104 mg, which was 5.86% of the total substance. Thus, the maximum amount of ME that remained in a sink condition was 1.775 mg. In its in vitro release, ME did not exceed 1.775 mg at any interval. The highest amount of ME released was 1.567 mg, indicating that ME remained in the sink condition.

Using two different pH values (5.5 and 7.4), we investigated the release of ME from niosomes with various ratios of S60 and cho (Figure 5). The amount of ME released from niosomes varied with pH. This revealed that ME-loaded niosomes loaded were pH sensitive. The amount of ME released decreased when the pH increased from 5.5 to 7.4. Thus, 85% of the ME released at a pH of 5.5 decreased to 70% at a pH of 7.4 within seven days. When administered to the wound, the minimal amount of ME released at a pH of 7.4, which corresponded to the pH of the blood, helped reduce side effects. Thus, the pH sensitivity of niosomes increased ME release on the skin surface (pH: 5.5). Compared with other ratios, the 2:1 ratio of S60 and cho (red line) allowed for a quicker ME release (Figure 5A) potentially because it had the lowest % EE (Figure 5B), resulting in more unencapsulated ME [77]. Additionally, increased surfactant structures in S60 delayed the release of ME from niosomes [78].

3.7. Swelling ratio characterization

When a dry film comes into contact with a moist wound surface, wound exudates are absorbed into the film matrix. This hydrate expands and transforms the film into a gel on the wound surface. This film expansion study aimed to assess the rate of wound dressing expansion (or hydration). A gelatin model was utilized to recreate the environment of a wet wound surface [79]. Figure 6A shows the percentage of film enlargement over time. The square-shaped films expanded in all directions and were finally converted into gels after a delayed hydration process on the gelatin surface. Hydration occurred more slowly in 1% SAP crosslinking than in 0.5% SAP crosslinking. After 30 min, SAP crosslinked with 0.5% and 1% Ca^{2+} progressively expanded to 867 and 1, 025% of their starting weights, respectively. These films expanded more quickly potentially due to their poor mechanical strength [80]. As such, long-term crosslinking with high Ca^{2+} concentrations changed the morphology of these patches. Fig. 6B-H shows that 0.5% Ca^{2+} crosslinking should last no more than 60 s, while 1% Ca^{2+} crosslinking should last no more than 30 s at a time. These results showed that crosslinking SAP with 1% Ca^{2+} for 30 s may preserve the form of the patches during wound dressing application, while undergoing a hydration process to maintain a moist wound bed environment. Extended use of a wound dressing that retains its structure and form is ideal for extremely exudative wounds [81].

3.8. Antibacterial study of ME-loaded niosomes incorporated in AP hydrogels

Bacterial infections are widely known to have increased wound exudates, which delay the wound-healing process [82]. Thus, an ideal

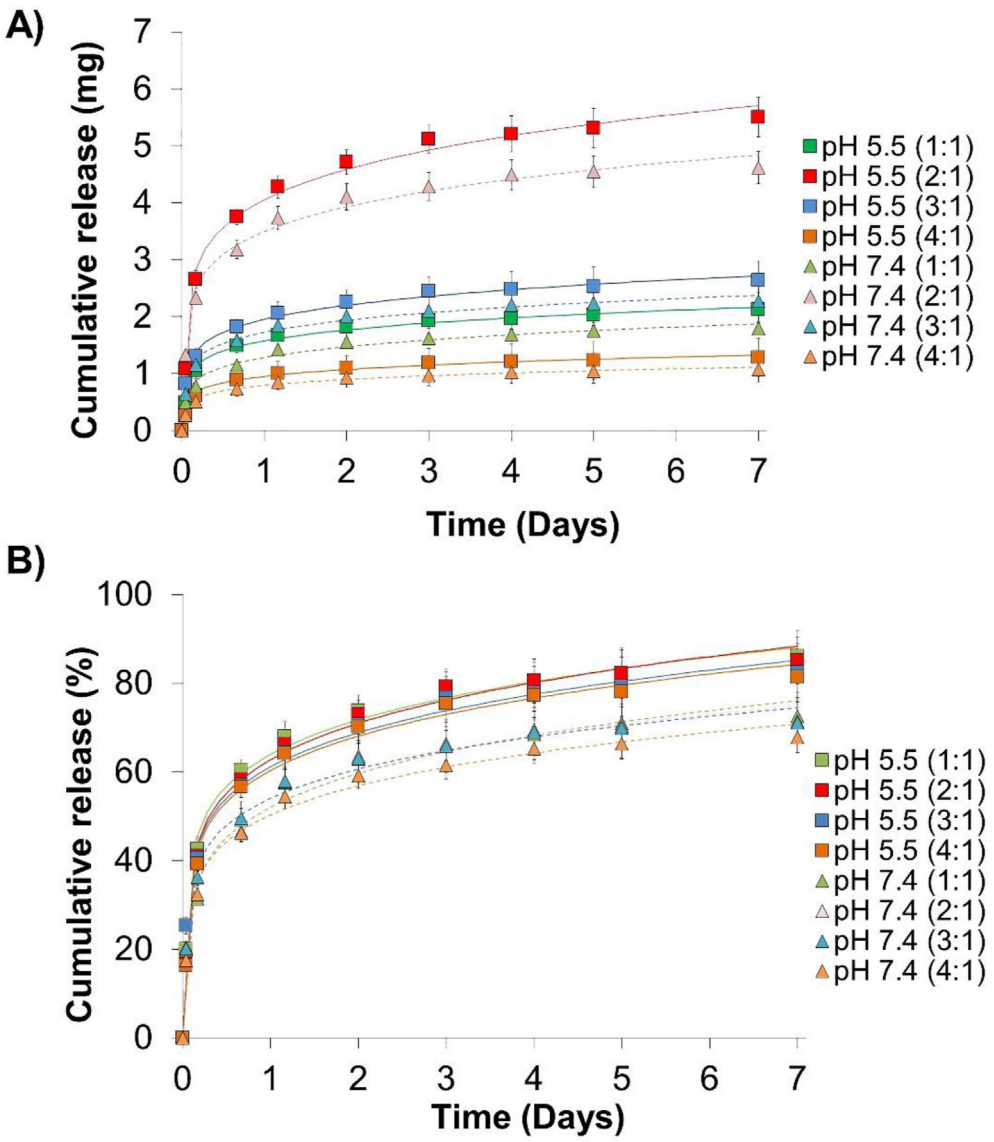

Figure 5. In vitro drug release profile of ME-loaded nanoparticles prepared using different ratios of S60 and cholesterol; 2:1 (red), 3:1 (blue), 4:1 (green), and 5:1 (orange) at a pH of 5.5 (square) and 2:1 (red), 3:1 (blue), 4:1 (green), and 5:1 (orange) at a pH of 7.4 (triangle) shown mg (A), and percent (B).

wound dressing material should have potent antibacterial capabilities to accelerate wound healing by lowering the number of microorganisms and decreasing the inflammatory response of wounds [83]. In this study, we conducted a test to determine the antibacterial activity of ME released from niosomes in SAP patches (Figure 7A and 7B) against *S. aureus* and *S. epidermidis*. Antibacterial activity was determined using 10^5 CFU/mL bacterial suspensions. Based on these findings, the most effective patches were those that comprised 1 part ME and were placed in niosomes with a 2:1 ratio of S60 and cho and then crosslinked with 1% AP for 30 s. A 1:1 ratio of ME and culture media inhibited (>90 percent) *S. aureus* and *S. epidermidis* for up to 4.5 days (Figures 7C and 7D). This indicated that the antibacterial action of the ME released significantly decreased over time. Nevertheless, the ME concentration increased, enabling the effective suppression of both bacteria. Additionally, while an excessive amount of ME inhibits bacteria, it may have a detrimental impact on normal cells as well.

The antibacterial activity of the SAP dressings incorporated with ME-loaded niosomes (Figure 8A) was determined by calculating the ZOIs around the patches. On culture plates inoculated with *S. aureus* and *S. epidermidis*, wound dressing patches with medium (15 mg) and high doses (20 mg) showed consistent bacterial growth inhibition (Figure 8B) and thus sustained antibacterial activities. After one day of incubation, the ZOIs surrounding the wound dressing patches were observed. As demonstrated by narrower ZOIs, a medium dose of ME-loaded niosomes incorporated into SAP patches showed a less effective antibacterial activity than that those with a high dose.

3.9. Cell viability assay

Biocompatibility testing of medical products and devices is critical to ensure their safe use, particularly in patients. The biocompatibility of the patches was in terms of cytotoxicity (in vitro cell culture model), hemocompatibility, and skin irritation (animal model). Cytotoxicity testing is critical for wound-dressing patches [84]. In vitro cytotoxicity may illustrate the presence of changes inside cells, ranging from cell death to minor changes in some cellular activities. An MTT assay is often

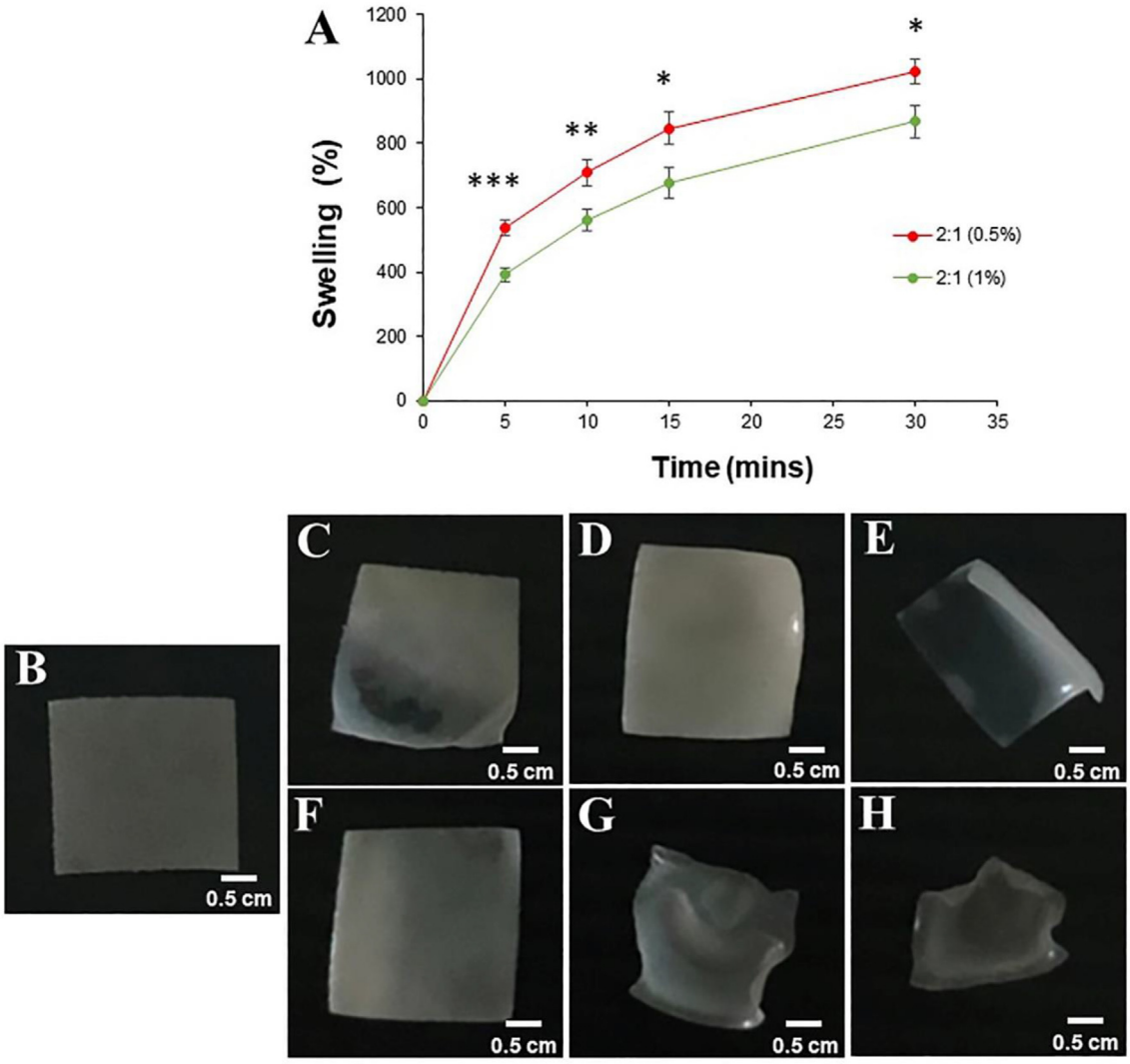

Figure 6. (A) Swelling curves of wound dressings containing a 2:1 ratio of alginate and pectin crosslinked with 0.5% (red) and 1% (green) $CaCl_2$ in PBS with a pH of 7.4. *P < 0.05, **P < 0.01, and ***P < 0.005 compared at the same time points. Physical appearance of AP hydrogel films at $CaCl_2$ concentrations of 0.5% (C, D, and E) and 1% (F, G, and H) and time intervals of 30 (C and F), 60 (D and G), and 90 (E and H) min compared with that of control without crosslinking (B).

used to determine in vitro cytotoxicity because it is a rapid and efficient approach to determine mitochondrial dysfunction that correlates well with cell growth. It is based on the use of tetrazolium salt MTT, which may be transformed into an insoluble blue formazan product by mitochondrial enzymes in live cells [85]. The L929 cell line is frequently used to assess the cytotoxicity of medical devices according to ISO 10993–5 [86]. Therefore, we used the L929 cell line as an in vitro model for cytotoxicity assays. Figure 9A shows the corresponding cytotoxic effects on cell viability and morphology. Both low- and medium-dose patches had no cytotoxic effects, exhibiting good cell viability (>80%) for all extract concentrations. Additionally, Figures 9B-9S, except for 9C, shows no significant alteration in the morphology of L929 cells after a 24-h culture in DMEM supplemented with patch extracts. While high-dose patches (20 mg) influenced L929 survival, cell survival was <80% at 100% and 50% DMEM extraction. Therefore, low- (10 mg) and medium-dose (15 mg) wound dressings are optimal because these do not inhibit fibroblast growth.

3.10. Cell morphology study

SEM images were taken to study cell adherence to the patches Cell proliferation and filopodia were observed. For the low- (Figure 10C) and medium-dose (Figure 10D) patches, the cells adhered to the patches and were distributed compared to glass coverslip (Figure 10A) and blank hydrogel (Figure 10B). However, due to their large size, fibroblasts cannot enter the pore cavity and attached to the patches' surface. Fibroblasts produce and arrange the ECM, which is critical for lesion healing, and prevent the development of hypertrophic scars and keloids [87, 88]. For the high-dose patches (Figure 10E), fibroblast development was inhibited. Additionally, the cells remained spherical and lacked filopodia, indicating the patches' non-cytocompatibility [89]. This was due to ME's toxicity at higher concentrations. Therefore, we recommend the use of medium-dose (15 mg) patches.

3.11. Cell migration

Figure 11 illustrates the results of the in vitro cell migration test. After a 24-hour incubation period, approximately 20.63 ± 0.08% of the damaged area healed using the bare patch due to the migration and proliferation of L929 cells into the scratched region. Compared to those treated with a bare patch, cells treated with low- (26.68 ± 1.02), medium- (49.99 ± 0.13), or high-dose patches (43.07 ± 1.61) had a statistically significant ($p < 0.05$) improvement in wound closure. A significant difference in wound contraction was observed in the low-

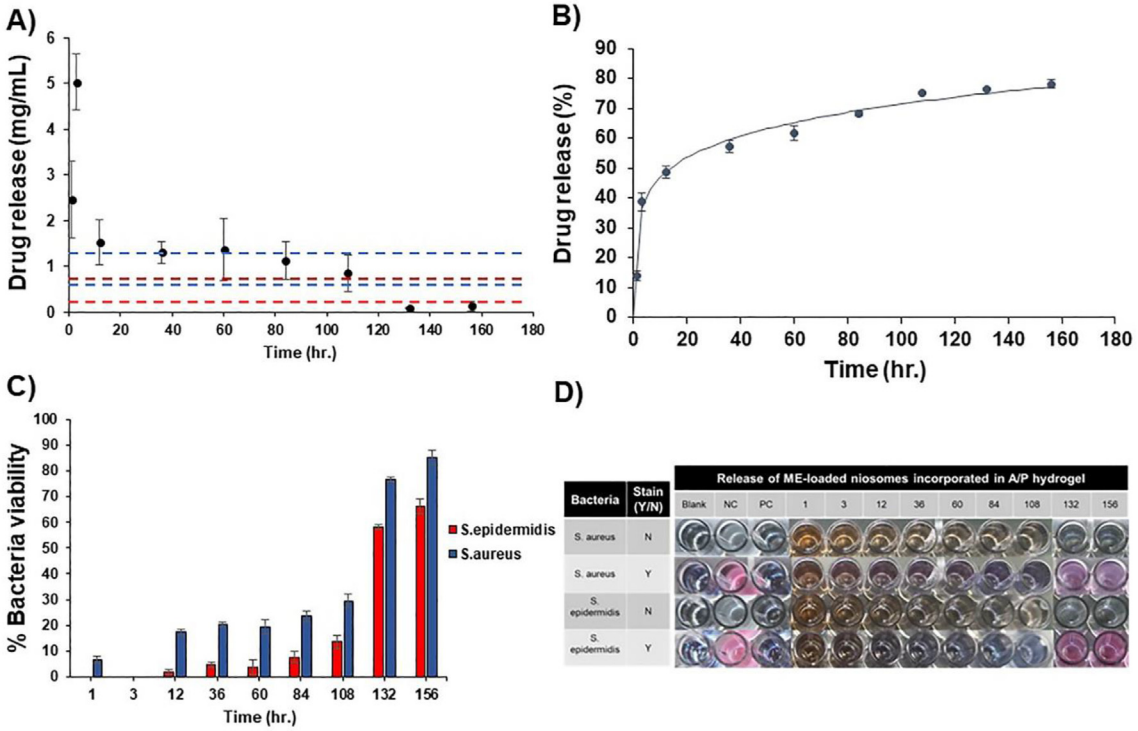

Figure 7. In vitro drug release of ME (A) Concentration of ME release in mg/mL and B) percentage of cumulative drug release (C) Percentage of bacterial viability after exposure according to ME release at various time points (D) Resazurin test after the exposure according to drug release at specified time intervals.

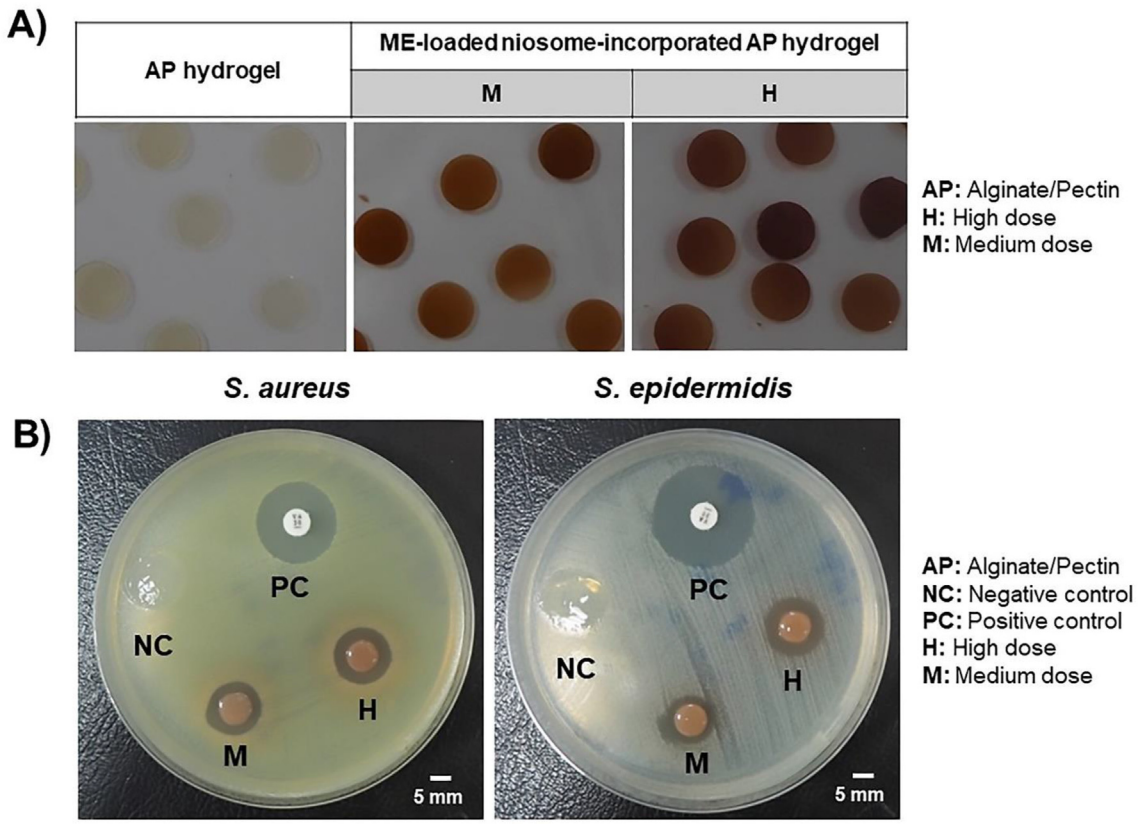

Figure 8. (A) Physical appearance of a wound dressing (B) Disk diffusion (ZOI) results of a wound dressing containing medium- (15 mg) and high- (20 mg) doses of ME for bacterial inhibition.

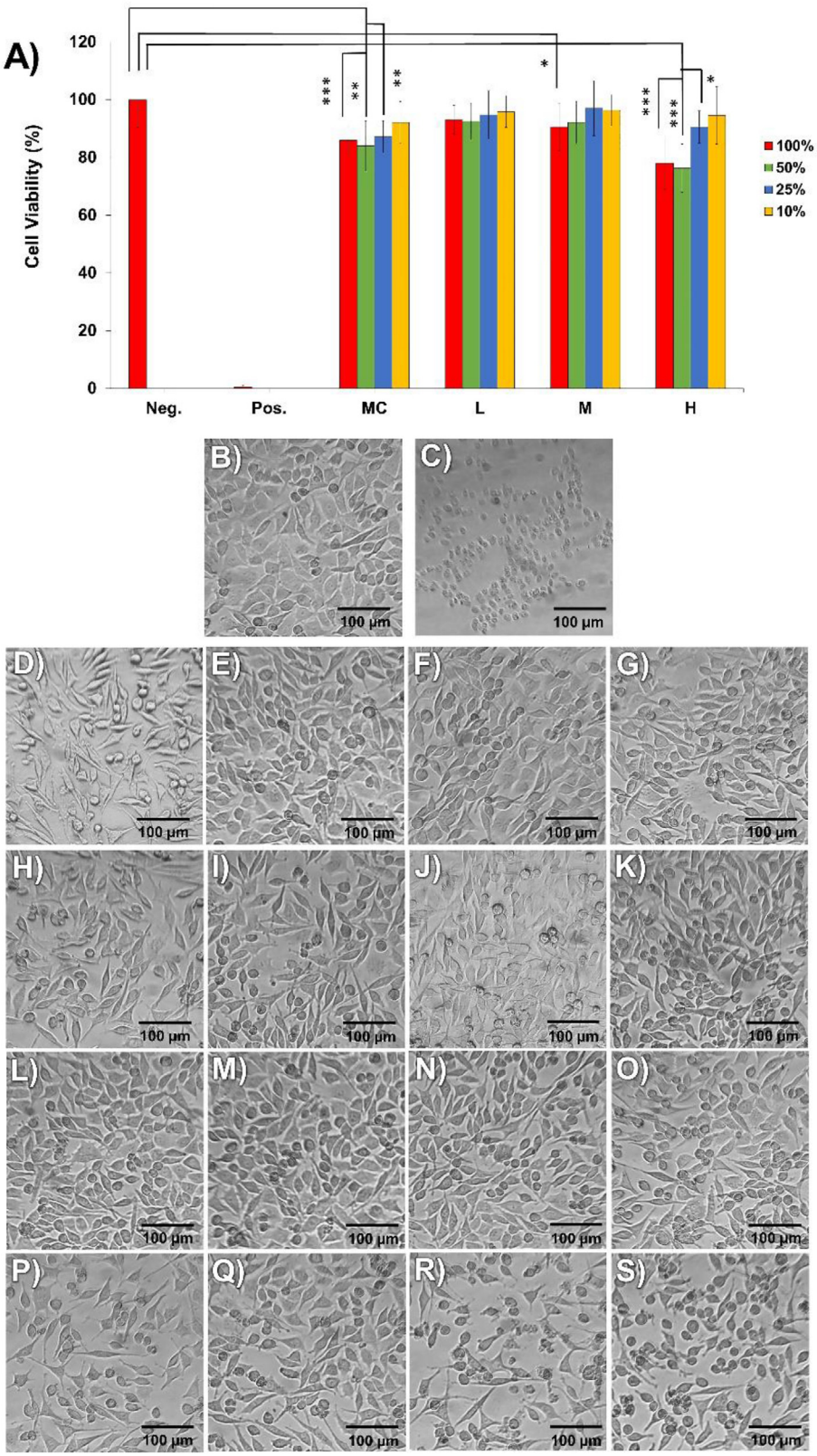

Figure 9. (A) Histograms representing the percentage, with respect to the NC (100%), of viable cells after exposure to wound dressings containing 0 mg (MC), 10 mg (L), 15 mg (M), and 20 mg (H) ME. *P < 0.05, **P < 0.01, and ***P < 0.005 compared with the NC. Morphology of L929 cells treated with DMEM as the NC (B), 1% Triton X-100 as the PC (C), and after exposure to various extractions from 100% (P, Q, R, and S) at the bottom to 10% at the top (D, E, F, and G) and different samples at 0 mg (MC) (D, H, L and P), 10 mg (E, I, M, and Q), 15 mg (F, J, N, and R), and 20 mg (G, K, O, and S). Scale bars = 100 µm.

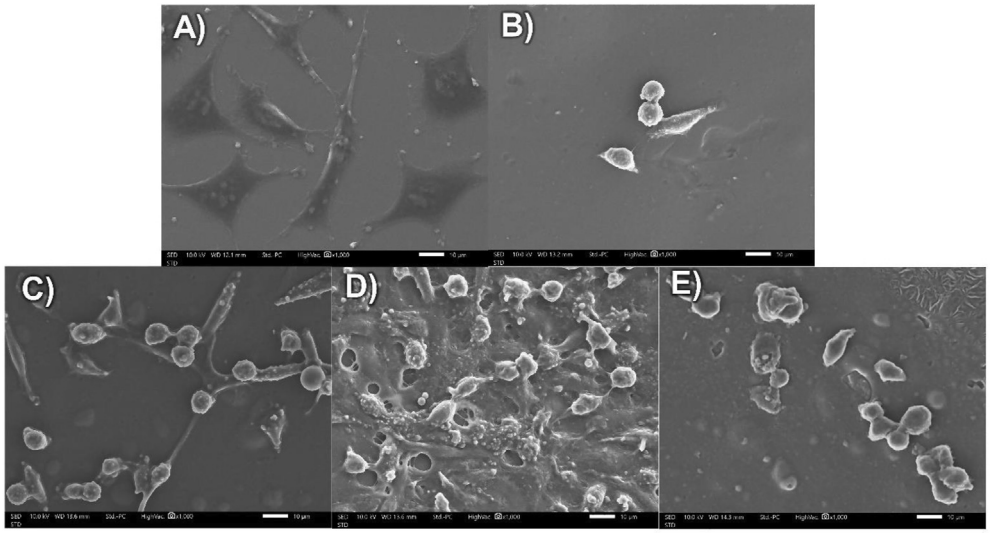

Figure 10. SEM image of L929 cells adhered to a glass coverslip (A), hydrogels with 0 mg (B), 10 mg (C), 15 mg (D), and 20 mg ME (E). Scale bars = 10 μm.

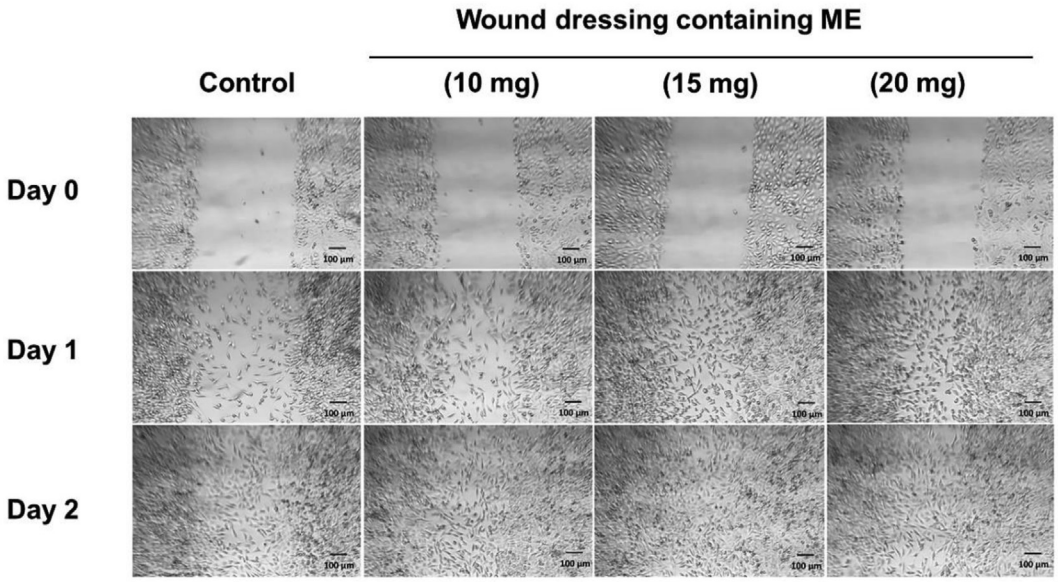

Figure 11. Effect of wound dressing containing ME on L929 cell migration. Scale bars = 100 μm.

dose patch compared with the bare patch. Further, compared to the low-dose patch, medium- and high-dose patches have a higher therapeutic efficacy. However, at 48 h, L929 cells treated with a medium-dose patch demonstrated a significantly greater wound healing ($p < 0.05$) than other types of patches. Interestingly, scratched regions treated with a medium-dose patch demonstrated a faster wound closure rate (97.79 ± 1.53).

3.12. Hemocompatibility

A hemolysis experiment was performed to determine the blood compatibility of SAP patches with various ME dosages. Blood compatibility is a critical for the development of substances for biomedical use. When RBCs come into contact with the extract, they swelled and burst due to the subsequent release of adenosine diphosphate. Adenosine diphosphate synthesis promotes platelet aggregation and accelerates blood clotting and thrombus formation [90]. Hemolysis, platelet adhesion, and blood clotting are distinct stages of the same process. Figures 12A–12D shows that all patches, except for the high-dose patch (Figure 12 E), with harmful RBCs were non-hemolytic. We used NSS as the NC. Due of its non-hemolytic action, a medium-dose patch has a potential in wound dressing application.

3.13. In vivo study

Using albino rabbits, we evaluated skin irritation in SAP patches incorporated with niosomes loaded with medium-dose ME [91]; the results are summarized in Table 6. Skin irritation is a localized inflammatory response that occurs immediately after stimulation. It is characterized by the development of acute inflammatory reactions clinically identified as erythema (redness), edema (swelling), itching, and discomfort [92]. Erythema and edema grading scales were used to rate the severity of skin irritation. The scores were as follows: 0 = none, 1 = slight erythema/slight edema (hardly visible), 2 = clearly visible/slight

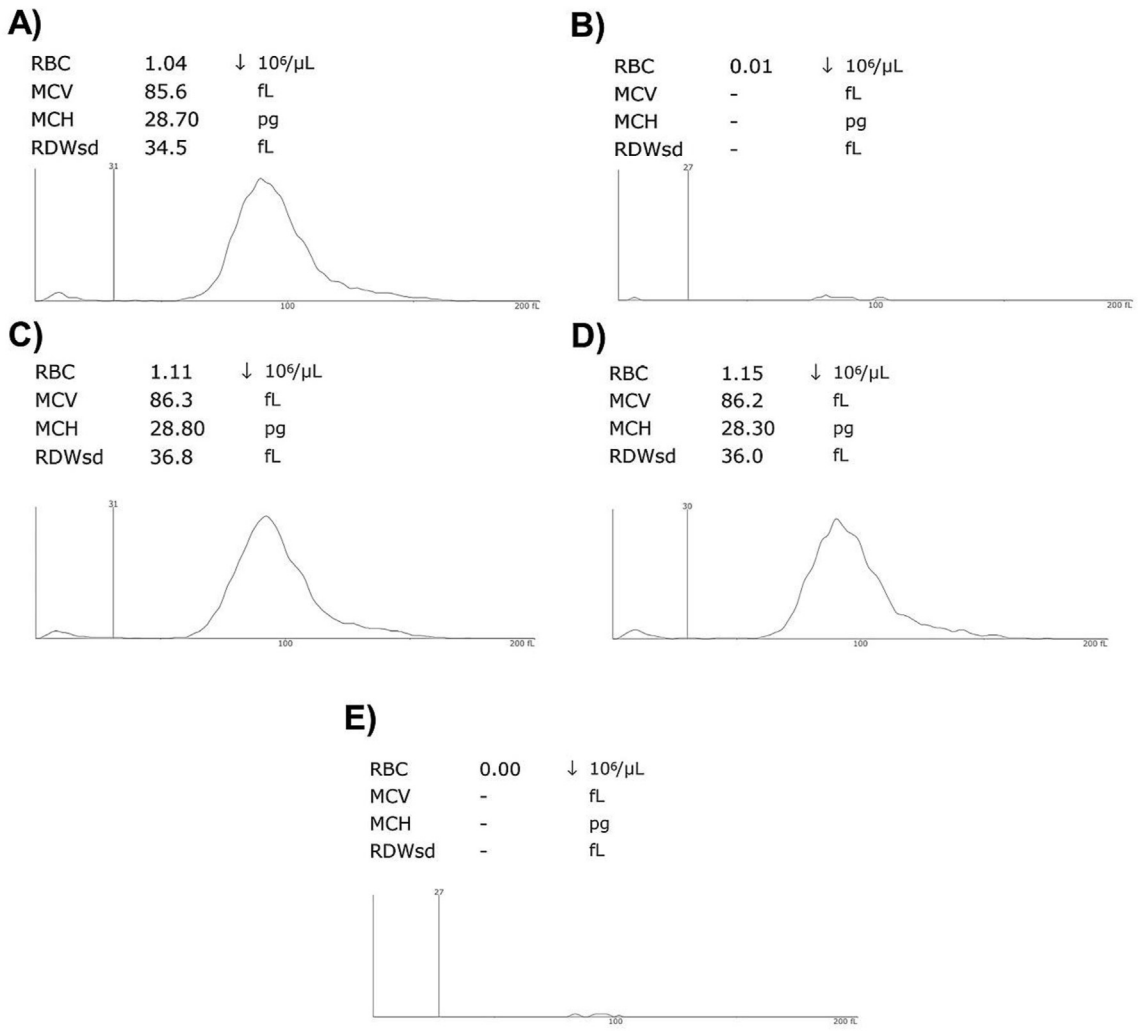

Figure 12. RBC histogram from the hemolytic activity test of (A) the NC (normal saline) (B) PC (distilled water), and wound dressings containing (C) 10 mg (D) 15 mg, and (E) 20 mg ME.

Table 7. Responsive scores of skin irritation.

Skin responses	Time (Hrs)	Score		
		Rabbit 1	Rabbit 2	Rabbit 3
Erythema	1	1	1	1
	24	0	1	1
	48	0	0	0
	72	0	0	0
Oedema	1	1	1	0
	24	0	0	0
	48	0	0	0
	72	0	0	0
Primary irritation index (PII)		PII = 2/8 = 0.25	PII = 3/8 = 0.38	PII = 2/8 = 0.25
Average Primary irritation index = (0.25 + 0.38+0.25)/3 = 0.29				

Data of mean ± SD of 3 independent experiments.

edema, 3 = moderate erythema/1-mm raised skin, 4 = serious erythema (dark red)/swelling even beyond the patch area. Table 7 shows no evidence of erythema or edema 72 h after applying medium-dose patches to the skin of the albino rabbits. All data revealed a favorable reaction in terms of skin irritation. Thus, the animal model experiments demonstrated that the SAP patches were biocompatible and had no harmful effects on skin cells.

4. Conclusion

Due to the high percentage of drug loading, yield, and encapsulation in niosomes with a 2:1 ratio of S60 and cho, the ratio was selected to encapsulate ME for wound dressing. The SAP patch incorporated with niosomes loaded with a medium-dose of ME demonstrated a high water absorption rate, which served as an effective barrier against bacterial penetration. Additionally, these patches generally exhibited a negative influence on cytotoxicity and skin irritation in vitro cell culture and in vivo models. Thus, we concluded that the patches are human/animal-friendly biomaterials with a significant biomedical application potential. It may be useful for burn skin therapy and as wound dressing materials. Although these patches are effective, a more detailed research on wound healing is needed before moving on to clinical trials. Nevertheless, this patch-fabrication technology involved loading active compounds into niosomes, which were then added into AP patches. Thus, this may be a key model for the creation of hydrogel patches. In the future, newly discovered novel compounds can be incorporated into this technology.

Declarations

Author contribution statement

Komgrit Eawsakul: Conceived and designed the experiments; Performed the experiments; Analysed and interpreted; Contributed reagents, materials, analysis tools or data; Wrote the paper.

Tassanee Ongtanasup: Conceived and designed the experiments; Performed the experiments; Analysed and interpreted the data; Wrote the paper.

Jitbanjong Tangpong: Conceived and designed the experiments; Wrote the paper.

Philaslak Pooprommin: Performed the experiments; Analysed and interpreted the data; Wrote the paper.

Chawan Manaspon: Performed the experiments; Analysed and interpreted the data; Contributed reagents, materials, analysis tools or data; Wrote the paper.

Smith Wanmasae: Performed the experiments; Analysed and interpreted the data; Wrote the paper.

Surat Sangkaew: Contributed reagents, materials, analysis tools or data.

Anisha Mazumder: Contributed reagents, materials, analysis tools or data; Wrote the paper.

Anupma Dwivedi: Contributed reagents, materials, analysis tools or data; Wrote the paper.

Funding statement

Komgrit Eawsakul was supported by Walailak University, Thailand [WU-IRG-64-034].

Data availability statement

Data will be made available on request.

Declaration of interest's statement

The authors declare no conflict of interest.

Additional information

No additional information is available for this paper.

References

[1] H. Yousef, M. Alhajj, S. Sharma, Anatomy, Skin (Integument), Epidermis, StatPearls Publishing, Treasure Island (FL), 2021.
[2] S. Ghatak, E.V. Maytin, J.A. Mack, V.C. Hascall, I. Atanelishvili, R. Moreno Rodriguez, et al., Roles of proteoglycans and glycosaminoglycans in wound healing and fibrosis, Int. J. Cell Mol. Biol. 2015 (2015), 834893.
[3] P.A.J. Kolarsick, M.A. Kolarsick, C. Goodwin, Anatomy and Physiology of the Skin, J. Dermatol. Nurses Assoc. 3 (4) (2011) 203–213.
[4] W.K. Stadelmann, A.G. Digenis, G.R. Tobin, Impediments to wound healing, Am. J. Surg. 176 (2, Supplement 1) (1998) 39S–47S.
[5] K. Banno, M.C. Yoder, Tissue regeneration using endothelial colony-forming cells: promising cells for vascular repair, Pediatr. Res. 83 (1) (2018) 283–290.
[6] S. Guo, L.A. DiPietro, Factors affecting wound healing, J. Dent. Res. 89 (3) (2010) 219–229.
[7] L. Bacakova, J. Pajorova, M. Bacakova, A. Skogberg, P. Kallio, K. Kolarova, et al., Versatile application of nanocellulose: from industry to skin tissue engineering and wound healing, Nanomaterials 9 (2) (2019) 164.
[8] S. Cascone, G. Lamberti, Hydrogel-based commercial products for biomedical applications: a review, Int. J. Pharm. 573 (2020), 118803.
[9] J. Koehler, F.P. Brandl, A.M. Goepferich, Hydrogel wound dressings for bioactive treatment of acute and chronic wounds, Eur. Polym. J. 100 (2018) 1–11.
[10] S.G. Abd Alla, M. Sen, A.W.M. El-Naggar, Swelling and mechanical properties of superabsorbent hydrogels based on Tara gum/acrylic acid synthesized by gamma radiation, Carbohydr. Polym. 89 (2) (2012) 478–485.
[11] Moist wound healing with commonly available dressings, Adv. Wound Care 10 (12) (2021) 685–698.
[12] M. Zhang, S. Chen, L. Zhong, B. Wang, H. Wang, F. Hong, Zn2+-loaded TOBC nanofiber-reinforced biomimetic calcium alginate hydrogel for antibacterial wound dressing, Int. J. Biol. Macromol. 143 (2020) 235–242.
[13] R. Gheorghita Puscaselu, A. Lobiuc, M. Dimian, M. Covasa, Alginate: from food industry to biomedical applications and management of metabolic disorders, Polymers 12 (10) (2020) 2417.
[14] D.R. Sahoo, T. Biswal, Alginate and its application to tissue engineering, SN Appl. Sci. 3 (1) (2021) 30.
[15] T. Ramdhan, S.H. Ching, S. Prakash, B. Bhandari, Physical and mechanical properties of alginate based composite gels, Trends Food Sci. Technol. 106 (2020) 150–159.
[16] S. Galus, A. Lenart, Development and characterization of composite edible films based on sodium alginate and pectin, J. Food Eng. 115 (4) (2013) 459–465.
[17] X. Wu, H. Sun, Z. Qin, P. Che, X. Yi, Q. Yu, et al., Fully physically crosslinked pectin-based hydrogel with high stretchability and toughness for biomedical application, Int. J. Biol. Macromol. 149 (2020) 707–716.
[18] M.A. Matica, F.L. Aachmann, A. Tøndervik, H. Sletta, V. Ostafe, Chitosan as a wound dressing starting material: antimicrobial properties and mode of action, Int. J. Mol. Sci. 20 (23) (2019) 5889.
[19] J. Pedraza-Chaverri, N. Cárdenas-Rodríguez, M. Orozco-Ibarra, J.M. Pérez-Rojas, Medicinal properties of mangosteen (Garcinia mangostana), Food Chem. Toxicol. 46 (10) (2008) 3227–3239.
[20] N. Tatiya-aphiradee, W. Chatuphonprasert, K. Jarukamjorn, Anti-inflammatory effect of Garcinia mangostana Linn. pericarp extract in methicillin-resistant Staphylococcus aureus-induced superficial skin infection in mice, Biomed. Pharmacother. 111 (2019) 705–713.
[21] K. Nakatani, M. Atsumi, T. Arakawa, K. Oosawa, S. Shimura, N. Nakahata, et al., Inhibitions of histamine release and prostaglandin E_2 synthesis by mangosteen, a Thai medicinal plant, Biol. Pharm. Bull. 25 (9) (2002) 1137–1141.
[22] O. Guillaume, X. Garric, J.-P. Lavigne, H. Van Den Berghe, J. Coudane, Multilayer, degradable coating as a carrier for the sustained release of antibiotics: preparation and antimicrobial efficacy in vitro, J. Contr. Release 162 (3) (2012) 492–501.
[23] D. Ag Seleci, M. Seleci, J.-G. Walter, F. Stahl, T. Scheper, Niosomes as nanoparticular drug carriers: fundamentals and recent applications, J. Nanomater. 2016 (2016), 7372306.
[24] S. Chen, S. Hanning, J. Falconer, M. Locke, J. Wen, Recent advances in non-ionic surfactant vesicles (niosomes): fabrication, characterization, pharmaceutical and cosmetic applications, Eur. J. Pharm. Biopharm. 144 (2019) 18–39.
[25] R. Rajera, K. Nagpal, S.K. Singh, D.N. Mishra, Niosomes: a controlled and novel drug delivery system, Biol. Pharm. Bull. 34 (7) (2011) 945–953.
[26] S. Kaderli, C. Boulocher, E. Pillet, D. Watrelot-Virieux, A.L. Rougemont, T. Roger, et al., A novel biocompatible hyaluronic acid–chitosan hybrid hydrogel for osteoarthrosis therapy, Int. J. Pharm. 483 (1) (2015) 158–168.
[27] M.H. Satari, E. Apriyanti, H.D.A. Dharsono, D. Nurdin, M. Gartika, D. Kurnia, Effectiveness of bioactive compound as antibacterial and anti-quorum sensing agent from myrmecodia pendans, An In Silico Study 26 (9) (2021) 2465.
[28] J. Hudzicki, Kirby-Bauer disk diffusion susceptibility test protocol, American society for microbiology 15 (2009) 55–63.
[29] A.A. Owayss, K. Elbanna, J. Iqbal, H.H. Abulreesh, S.R. Organji, H.S.A. Raweh, et al., In vitro antimicrobial activities of Saudi honeys originating from Ziziphus spina-christi L. and Acacia gerrardii Benth, Trees (Berl.) 8 (1) (2020) 390–401.
[30] E.P. Padla, L.T. Solis, R.M. Levida, C.-C. Shen, C.Y. Ragasa, Antimicrobial isothiocyanates from the seeds of moringa oleifera lam, %J Zeitschrift für Naturforschung C. 67 (11-12) (2012) 557–564.
[31] M.A. Pfaller, D.J. Diekema, Progress in antifungal susceptibility testing of Candida spp, Use of Clinical and Laboratory Standards Institute Broth Microdilution Methods 50 (9) (2012) 2846–2856.
[32] H.A.J. Hibbard, M.M. Reynolds, Fluorescent nitric oxide donor for the detection and killing of Pseudomonas aeruginosa, J. Mater. Chem. B 7 (12) (2019) 2009–2018.
[33] B.H. Neufeld, M.J. Neufeld, A. Lutzke, S.M. Schweickart, M.M. Reynolds, Metal–organic framework material inhibits biofilm formation of Pseudomonas aeruginosa, Adv. Funct. Mater 27 (34) (2017), 1702255.
[34] L.K. Yeo, C.S. Chaw, A.A. Elkordy, The effects of hydration parameters and Co-surfactants on methylene blue-loaded niosomes prepared by the thin film, Hydration Method 12 (2) (2019) 46.
[35] M. Danaei, M. Dehghankhold, S. Ataei, F. Hasanzadeh Davarani, R. Javanmard, A. Dokhani, et al., Impact of particle size and polydispersity index on the clinical applications of lipidic, Nanocarrier Systems 10 (2) (2018) 57.
[36] A. Sze, D. Erickson, L. Ren, D. Li, Zeta-potential measurement using the Smoluchowski equation and the slope of the current–time relationship in electroosmotic flow, J. Colloid Interface Sci. 261 (2) (2003) 402–410.
[37] P. García-Manrique, E. Serrano-Pertierra, E. Lozano-Andrés, S. López-Martín, M. Matos, G. Gutiérrez, et al., Selected tetraspanins functionalized niosomes as potential standards for exosome immunoassays, Nanomaterials 10 (5) (2020) 971.
[38] K. Eawsakul, P. Chinavinijkul, R. Saeeng, A. Chairoungdua, P. Tuchinda, N. Nasongkla, Preparation and characterizations of RSPP050-loaded polymeric micelles using poly (ethylene glycol)-b-poly (ε-caprolactone) and poly (ethylene glycol)-b-poly (D, L-lactide), Chem. Pharm. Bull. 65 (6) (2017) 530–537.
[39] N. Nasongkla, P. Tuchinda, B. Munyoo, K. Eawsakul, Preparation and characterization of MUC-30-loaded polymeric micelles against MCF-7 cell lines using molecular docking methods and in vitro study, Evid. base Compl. Alternative Med. (2021) 2021.
[40] C. Ingallina, F. Rinaldi, A. Bogni, J. Ponti, D. Passeri, M. Reggente, et al., Niosomal approach to brain delivery: development, characterization and in vitro toxicological studies, Int. J. Pharm. 511 (2) (2016) 969–982.

[41] A. Dwivedi, A. Mazumder, N. Nasongkla, Layer-by-layer nanocoating of antibacterial niosome on orthopedic implant, Int. J. Pharm. 547 (1-2) (2018) 235–243.

[42] N. Wongsuwan, A. Dwivedi, S. Tancharoen, N. Nasongkla, Development of dental implant coating with minocycline-loaded niosome for antibacterial application, J. Drug Deliv. Sci. Technol. 56 (2020), 101555.

[43] N. Sharmin, I. Sone, J.L. Walsh, M. Sivertsvik, E.N. Fernández, Effect of citric acid and plasma activated water on the functional properties of sodium alginate for potential food packaging applications, Food Packag. Shelf Life 29 (2021), 100733.

[44] B.A. Aderibigbe, B. Buyana, Alginate in Wound Dressings, Pharmaceutics 10 (2) (2018) 42.

[45] A.A. Mahmoud, A.H. Salama, Norfloxacin-loaded collagen/chitosan scaffolds for skin reconstruction: preparation, evaluation and in-vivo wound healing assessment, Eur. J. Pharmaceut. Sci. 83 (2016) 155–165.

[46] S. Wang, O.-H. Kang, D.-Y. Kwon, Trans-Cinnamaldehyde Exhibits Synergy with Conventional Antibiotic against Methicillin-Resistant Staphylococcus aureus, Int. J. Mol. Sci. 22 (5) (2021) 2752.

[47] S. Srisang, N. Nasongkla, Layer-by-layer dip coating of Foley urinary catheters by chlorhexidine-loaded micelles, J. Drug Deliv. Sci. Technol. 49 (2019) 235–242.

[48] C. Thedrattanawong, C. Manaspon, N. Nasongkla, Controlling the burst release of doxorubicin from polymeric depots via adjusting hydrophobic/hydrophilic properties, J. Drug Deliv. Sci. Technol. 46 (2018) 446–451.

[49] M.J. Talbot, R.G. White, Methanol fixation of plant tissue for Scanning Electron Microscopy improves preservation of tissue morphology and dimensions, Plant Methods 9 (1) (2013) 36.

[50] X. Li, X. Ji, K. Chen, M.W. Ullah, X. Yuan, Z. Lei, et al., Development of finasteride/PHBV@polyvinyl alcohol/chitosan reservoir-type microspheres as a potential embolic agent: from in vitro evaluation to animal study, Biomater. Sci. 8 (10) (2020) 2797–2813.

[51] A.I. Sokolova, E.R. Pavlova, Y.V. Khramova, D.V. Klinov, K.V. Shaitan, D.V. Bagrov, Imaging human keratinocytes grown on electrospun mats by scanning electron microscopy, Microsc. Res. Tech. 82 (5) (2019) 544–549.

[52] S. Martinotti, E. Ranzato, Scratch wound healing assay, in: K. Turksen (Ed.), Epidermal Cells: Methods and Protocols, Springer US, New York, NY, 2020, pp. 225–229.

[53] A.V.P. Bobadilla, J. Arévalo, E. Sarró, H.M. Byrne, P.K. Maini, T. Carraro, et al., *In vitro* cell migration quantification method for scratch assays, J. R. Soc. Interface 16 (151) (2019), 20180709.

[54] K. Eawsakul, S. Tancharoen, N. Nasongkla, Combination of dip coating of BMP-2 and spray coating of PLGA on dental implants for osseointegration, J. Drug Deliv. Sci. Technol. 61 (2021), 102296.

[55] S. Srisang, A. Boongird, M. Ungsurungsie, P. Wanasawas, N. Nasongkla, Biocompatibility and stability during storage of Foley urinary catheters coated chlorhexidine loaded nanoparticles by nanocoating: in vitro and in vivo evaluation, J. Bio. Mater. Res. Part B: Appl. Bio. 109 (4) (2021) 496–504.

[56] OECD, OECD Guidelines for the Testing of Chemicals, Organization for Economic, 1994.

[57] T. Reid, C. Kashangura, C. Chidewe, M.A. Benhura, B. Stray-Pedersen, T. Mduluza, Characterization of Anti−Salmonella *typhi* compounds from medicinal mushroom extracts from Zimbabwe, Int. J. Med. Mushrooms 21 (7) (2019) 713, 24.

[58] C. Chepkirui, K.T. Yuyama, L.A. Wanga, C. Decock, J.C. Matasyoh, W.-R. Abraham, et al., Microporenic acids A–G, biofilm inhibitors, and antimicrobial agents from the basidiomycete microporus species, J. Nat. Prod. 81 (4) (2018) 778–784.

[59] A.G. Granja, F. Carrillo-Salinas, A. Pagani, M. Gómez-Cañas, R. Negri, C. Navarrete, et al., A cannabigerol quinone alleviates neuroinflammation in a chronic model of multiple sclerosis, J. Neuroimmune Pharmacol. 7 (4) (2012) 1002–1016.

[60] D.H. Kim, E.K. Shin, Y.H. Kim, B.W. Lee, J.-G. Jun, J.H.Y. Park, et al., Suppression of inflammatory responses by celastrol, a quinone methide triterpenoid isolated from Celastrus regelii, Eur. J. Clin. Invest. 39 (9) (2009) 819–827.

[61] G.F. Vafina, A.I. Poptsov, L.V. Spirikhin, F.Z. Galin, Synthesis of new methoxyquinopimaric-acid scaffold derivatives, Chem. Nat. Compd. 54 (1) (2018) 88–91.

[62] J. Fan, H. Liu, J. Wang, J. Zeng, Y. Tan, Y. Wang, et al., Procyanidin B2 improves endothelial progenitor cell function and promotes wound healing in diabetic mice via activating Nrf2, J. Cell Mol. Med. 25 (2) (2021) 652–665.

[63] M. Kapoor, R. Howard, I. Hall, I. Appleton, Effects of epicatechin gallate on wound healing and scar formation in a full thickness incisional wound healing model in rats, Am. J. Pathol. 165 (1) (2004) 299–307.

[64] M. Muchtaridi, F.S. Afiranti, P.W. Puspasari, A. Subarnas, P.S. Susilawati, Research, Cytotoxicity of Garcinia mangostana L. pericarp extract, fraction, and isolate on HeLa cervical cancer cells, Y.J.J.o. J. Pharmaceut. Sci. Res. 10 (2) (2018) 348–351.

[65] G.S. Singhal, E. Rabinowitch, Changes in the absorption spectrum of methylene blue with pH, J. Phys. Chem. 71 (10) (1967) 3347–3349.

[66] X.-C. Huang, J.-K. Ma, S.-L. Wei, Preparation and application of a novel magnetic molecularly imprinted polymer for simultaneous and rapid determination of three trace endocrine disrupting chemicals in lake water and milk samples, Anal. Bioanal. Chem. 412 (8) (2020) 1835–1846.

[67] Y. Zhong, C. Ru, S. Wang, Z. Li, Y. Cheng, An online, non-destructive method for simultaneously detecting chemical, biological, and physical properties of herbal injections using hyperspectral imaging with artificial intelligence, Spectrochim. Acta Mol. Biomol. Spectrosc. 264 (2022), 120250.

[68] Y.S. Leong, P.J. Ker, M.Z. Jamaludin, S.M. Nomanbhay, A. Ismail, F. Abdullah, et al., UV-vis spectroscopy: A New Approach for Assessing the Color Index of Transformer Insulating Oil, Sensors 18 (7) (2018) 2175.

[69] R. Matias, P.R.S. Ribeiro, M.C. Sarraguça, J.A. Lopes, A UV spectrophotometric method for the determination of folic acid in pharmaceutical tablets and dissolution tests, Anal. Methods 6 (9) (2014) 3065–3071.

[70] Y. Soleimanian, S.A.H. Goli, J. Varshosaz, S.M. Sahafi, Formulation and characterization of novel nanostructured lipid carriers made from beeswax, propolis wax and pomegranate seed oil, Food Chem. 244 (2018) 83–92.

[71] K. Ruckmani, V. Sankar, Formulation and optimization of zidovudine niosomes, AAPS PharmSciTech 11 (3) (2010) 1119–1127.

[72] A.S. Nayak, S. Chodisetti, S. Gadag, U.Y. Nayak, S. Govindan, K. Raval, Tailoring solulan C24 based niosomes for transdermal delivery of donepezil: in vitro characterization, evaluation of pH sensitivity, and microneedle-assisted Ex vivo permeation studies, J. Drug Deliv. Sci. Technol. 60 (2020), 101945.

[73] Y. Hao, F. Zhao, N. Li, Y. Yang, K.a. Li, Studies on a high encapsulation of colchicine by a niosome system, Int. J. Pharm. 244 (1) (2002) 73–80.

[74] H. Hemachandran, A. Anantharaman, S. Mohan, G. Mohan, D.T. Kumar, D. Dey, et al., Unraveling the inhibition mechanism of cyanidin-3-sophoroside on polyphenol oxidase and its effect on enzymatic browning of apples, Food Chem. 227 (2017) 102–110.

[75] A. Farmoudeh, J. Akbari, M. Saeedi, M. Ghasemi, N. Asemi, A. Nokhodchi, Methylene blue-loaded niosome: preparation, physicochemical characterization, and in vivo wound healing assessment, Drug delivery translational research 10 (5) (2020) 1428–1441.

[76] S.K. Mehta, N. Jindal, Formulation of Tyloxapol niosomes for encapsulation, stabilization and dissolution of anti-tubercular drugs, Colloids Surf., B 101 (2013) 434–441.

[77] N.M. Desai, J. Gilbert Stanley, P.S. Murthy, Green coffee nanoparticles: optimisation, in vitro bioactivity and bio-release property, J. Microencapsul. 37 (1) (2020) 52–64.

[78] M. Gupta, B. Vaidya, N. Mishra, S.P. Vyas, Effect of surfactants on the characteristics of fluconazole niosomes for enhanced cutaneous delivery, Artif. Cell Blood Substit. Biotechnol. 39 (6) (2011) 376–384.

[79] W. Schuurman, P.A. Levett, M.W. Pot, P.R. van Weeren, W.J.A. Dhert, D.W. Hutmacher, et al., Gelatin-methacrylamide hydrogels as potential biomaterials for fabrication of tissue-engineered cartilage constructs, Macromol. Biosci. 13 (5) (2013) 551–561.

[80] K.Y. Lee, J.A. Rowley, P. Eiselt, E.M. Moy, K.H. Bouhadir, D.J. Mooney, Controlling mechanical and swelling properties of alginate hydrogels independently by cross-linker type and cross-linking density, Macromolecules 33 (11) (2000) 4291–4294.

[81] E.A. Kamoun, E.-R.S. Kenawy, X. Chen, A review on polymeric hydrogel membranes for wound dressing applications: PVA-based hydrogel dressings, J. Adv. Res. 8 (3) (2017) 217–233.

[82] Biofilms, Wounds, An Overview of the Evidence, Aesthetic Plast. Surg. 4 (7) (2015) 373–381.

[83] Q. Zeng, Y. Qian, Y. Huang, F. Ding, X. Qi, J. Shen, Polydopamine nanoparticle-dotted food gum hydrogel with excellent antibacterial activity and rapid shape adaptability for accelerated bacteria-infected wound healing, Bioact. Mater. 6 (9) (2021) 2647–2657.

[84] N. Roy, N. Saha, P. Humpolicek, P. Saha, Permeability and biocompatibility of novel medicated hydrogel wound dressings, Soft Mater. 8 (4) (2010) 338–357.

[85] J.C. Stockert, R.W. Horobin, L.L. Colombo, A. Blázquez-Castro, Tetrazolium salts and formazan products in Cell Biology: viability assessment, fluorescence imaging, and labeling perspectives, Acta Histochem. 120 (3) (2018) 159–167.

[86] V. Cannella, R. Altomare, V. Leonardi, L. Russotto, S. Di Bella, F. Mira, et al., In Vitro biocompatibility evaluation of nine dermal fillers on L929 cell line, BioMed Res. Int. 2020 (2020), 8676343.

[87] Extracellular matrix reorganization during wound healing and its impact on abnormal scarring, Adv. Wound Care 4 (3) (2015) 119–136.

[88] Extracellular matrix and dermal fibroblast function in the healing wound, Adv. Wound Care 5 (3) (2016) 119–136.

[89] S. Veziroglu, M. Ayna, T. Kohlhaas, S. Sayin, J. Fiutowski, Y.K. Mishra, et al., Marine algae incorporated polylactide acid patch: novel candidate for targeting osteosarcoma cells without impairing the osteoblastic proliferation, Polymers 13 (6) (2021) 847.

[90] R.M. Des Prez, S. Steckley, R.M. Stroud, J. Hawiger, Interaction of histoplasma capsulatum with human platelets, J. Infect. Dis. 142 (1) (1980) 32–39.

[91] A.V. Thanusha, V. Koul, Biocompatibility evaluation for the developed hydrogel wound dressing – ISO-10993-11 standards – in vitro and in vivo study, Biomed. Phy. Engin. Express 8 (1) (2021), 015010.

[92] N. Haridas, M.J. Rosemary, Effect of steam sterilization and biocompatibility studies of hyaluronic acid hydrogel for viscosupplementation, Polym. Degrad. Stabil. 163 (2019) 220–227.